Calcium isotope fractionation in solids (silicates, carbonates, oxides) from Density Functional Theory: superiority of the PBEsol functional, and vibrational dragging by strong anionic groups

Merlin Meheut, Vasileios Mavromatis, Magali Benoit, Jacques Schott

Calcium isotope fractionation in solids (silicates, carbonates, oxides) from Density Functional Theory: superiority of the PBEsol functional, and vibrational dragging by strong anionic groups.

Merlin Méheut[1,⋆], Vasileios Mavromatis
(Βασίλειος Μαυρομάτης) , Magali Benoît[2], and Jacques Schott[1]
[1] *GET, UMR 5563 UR 154 CNRS Université Paul-Sabatier IRD Observatoire Midi-Pyrénées 14 avenue Edouard Belin, 31400 Toulouse, France*
[2] *CEMES CNRS UPR 8011 29 rue Jeanne Marvig, 31055 Cedex Toulouse, France*
⋆ *corresponding author: merlin.meheut@get.omp.eu*

Abstract

The fractionation of Ca isotopes has been computed between various solids (calcite, dolomite, aragonite, lime CaO, diopside, grossular) based on six different DFT-based theoretical schemes (PZ, PBE, vdW-DF2, BLYP, BLYP + Grimme-D2 correction, and PBEsol). The results strongly depend on the selected theoretical scheme, with almost 2‰ differences in some cases, for isotope fractionations varying by 8‰ overall. Based on several quality criteria (accuracy and consistency of the error on structure and vibrations in particular), the PBEsol functional appears more accurate and more consistent than the others, with PZ and VdW-oriented functionals behaving particularly badly. The possibilities for correction based on experimental frequencies were evaluated in details, pushing further the principle of frequency rescaling. Even for exceptional cases where the experimental frequencies were exhaustively characterized, the uncertainty attached to this procedure reaches typically 0.5‰. Discrepancy with previously published results suggests that, beyond the selected theoretical scheme, numerical details such as electronic wave-function basis sets or general modelling approaches may also significantly infer on the result. Recommended values for the mineral-calcite Ca isotope fractionation at 300K are -0.9, -2.9, +2.3, +0.12 and +4.3‰ for dolomite, aragonite, lime CaO, diopside and grossular, respectively. The most important parameter controlling the fractionation of Ca isotopes appears to be the presence of strong anionic groups, inasmuch as those groups vibrate at high frequency and "drag" Ca in their vibrational displacements, inducing significant contributions to the isotope fractionation properties of this element. This is the case for SiO_4 tetrahedral groups. On the opposite, CO_3 vibrations in carbonates appear disconnected from Ca displacements, explaining the lighter values of carbonates compared to silicates.

1. INTRODUCTION

Calcium is the 5^{th} most abundant element in Earth's crust. It is also the 6^{th} most important macronutrient in plants, and one of the most important elements in human physiology. Variations of its stable isotope composition, measurable by recent progresses in mass spectrometry and analytical chemistry, bring major insights into the geochemical and physiological processes involving Ca, with application to e.g. climatic reconstruction, bone cancer diagnosis or design of efficient agricultural nutrients (Gussone et al., 2016). Ca isotopes have shown their potential to unravel processes occurring at the water-soil-plant interface (Schmitt, 2016), as well as during its transfer to oceans and within oceans (Gussone et al., 2016).

To extract the information contained in those signatures, constraints on isotopic fractionation induced by individual physico-chemical processes are mandatory. Equilibrium isotope fractionation is a key parameter and can be quantified from theoretical considerations based on statistical physics and electronic structure calculations. Efficient electronic structure calculations are made possible by the Density Functional Theory (DFT). Calcium isotope equilibrium fractionation has been explored by Antonelli et al. (2019) and Huang et al. (2019) for high temperature silicate systems, by Rustad et al. (2010) and Wang et al. (2017b) at low temperature, between carbonates (calcite, dolomite, magnesite) and aqueous Ca^{2+}, and by Colla et al. (2013) and Moynier and Fujii (2017) between various dissolved Ca species. However, it is difficult to infer the reliability of those studies. For example, Rustad et al. (2010) and Wang et al. (2017b) provide very different estimate of the calcite-dolomite equilibrium (2.1 vs 1.2 ‰ at 300K). A key aspect of validation is the comparison to experimental data (structure, vibrations, and possibly isotopes fractionation). In particular, calculated frequencies should be properly compared to experimental measurements. This requires exhaustive compilations of vibrational properties (from Raman and Infrared spectroscopies). The materials in this study were chosen as the most exhaustively characterized among the carbonate, silicate and oxide families. They all correspond to ionic, anhydrous, compact solids. The important cases (see below) of hydrous minerals (such as ikaite or Ca-oxalates) or dissolved species cannot be considered as they are insufficiently well characterized for their vibrational properties.

The core approximation that permits electronic structure calculations based on the density

functional theory resides in the approximate functional used to describe the way that electronic energy depends on electronic density. In that respect, an issue insufficiently addressed by the above mentioned studies is the effect of the theoretical scheme, and, central to it, the choice of the density functional. The simple local density approximation (LDA) is considered as suitable for silicates (e.g. Tsuchiya et al., 2004), but inadequate for materials with H-bonds, for which gradient-corrected approximation (GCA) are generally preferred (Lee et al., 1992, Hamann, 1997). The hybrid B3LYP functional has also been used by several studies to compute carbonate solids and dissolved species (e.g Rustad et al., 2010, Moynier and Fujii, 2017). Although not the main focus of this paper, Ca in solution is an important system to understand fractionations observed in nature, in particular for low-temperature systems, in which isotopic signatures generally result from precipitation in solution. Ca in solution seems better described (at least for its structure) by theoretical schemes including Van der Waals corrections (Baer and Mundy, 2016).

Fractionation properties are occurring between phases, that can belong to different families, better described by different theoretical schemes. However, because they ultimately originate from small differences in vibrational properties, it is very important to compute those properties as consistently as possible. One (quite satisfying) possibility is to keep the same theoretical scheme for all phases. In this goal, we evaluate the efficiency of six different theoretical schemes, among those described above. Another possibility is to correct the results of a particular scheme based on experiment. The most common approach (e.g. Schauble et al., 2006) is to consider that a given theoretical scheme biases frequencies by a constant relative amount at first order, and to take a single rescaling factor determined from the comparison with experiment to correct theoretical frequencies. The efficiency of such corrections has to be evaluated.

Various solids were considered in this work (oxides: lime CaO; carbonates: calcite $CaCO_3$, dolomite $CaMg(CO_3)_2$, aragonite $CaCO_3$; silicates: grossular $Ca_3Al_2Si_4O_{12}$, diopside $CaMgSi_2O_6$), chosen for their structural variety, and most importantly for the existence of exhaustive quantification of their vibrational properties at the experimental level. Structures with H-bonds are absent from this list, as the more suitable ones (such as ikaite or Ca-oxalates) remain partly characterized for their vibrational properties. The structural, vibrational and fractionation properties of these materials are calculated with various theoretical schemes (PZ, PBE, vdW-DF2, BLYP, BLYP+D2, PBEsol). The code that is used

here (Quantum Espresso) cannot implement the B3LYP functional efficiently, due to the use of plane wave basis sets, and the efficiency of this functional was only estimated based on literature. The PBEsol functional (Perdew et al., 2008) previously showed efficient in the challenging case of the aragonite-calcite equilibrium (Demichelis et al., 2017). For the sake of a precise comparison with the work of Rustad et al., 2010, we also computed calcite properties within the BP86 functional (Becke, 1988, Perdew, 1986), that is similar to PBE or BLYP .

2. METHODS

2.1. The Isotopic Fractionation Factor α.

$\beta^{44/40}Ca_A$ is the isotopic fractionation factor of the element Ca between the phase A and a perfect gas of Ca atoms, having the natural mean isotopic concentration. The isotopic fractionation factor $\alpha^{44/40}Ca_{A-B}$ relative to an atom Ca, between two phases A and B can be written as the ratio of the β-factors relative to this atom and to each phase separately (Richet et al., 1977).

If A is a crystalline solid, $\beta^{44/40}Ca_A$ can be computed from the harmonic vibrational properties of A using

$$\beta^{44/40}Ca_A = \left[\frac{Q(^{44}Ca_N)}{Q(^{40}Ca_N)}\right]^{1/N} \left[\frac{m_{40}}{m_{44}}\right]^{3/2} \tag{1}$$

where $Q(^{44}Ca_N)$ and $Q(^{40}Ca_N)$ are the partition functions of the system having all the N Ca atoms substituted by ^{44}Ca and ^{40}Ca, respectively. The harmonic partition function of a crystalline solid is:

$$Q = \left[\prod_{i=1}^{3N^{at}} {\prod_{\{\boldsymbol{q}\}}}^{*} \frac{e^{-h\nu_{\boldsymbol{q},i}/(2kT)}}{1-e^{-h\nu_{\boldsymbol{q},i}/(kT)}}\right]^{1/(N_q)} \tag{2}$$

where $\nu_{\mathbf{q},i}$ are the frequencies of the phonon with wavevector $\mathbf{q}$ and branch index i=1,3N^{at}. N^{at} is the number of atoms in the unit cell, N is the number of Ca atoms in the unit cell, T is the absolute temperature, k is the Boltzmann constant and h is Plank's constant. The product is performed on a sufficiently large grid of N_q $\boldsymbol{q}$-vectors in the Brillouin zone. The

97 ⋆ symbol above the product of Eq. (2) indicates that the three translational modes with
98 $\nu_{\mathbf{0},i} = 0$ are not considered.

99 2.2. Vibrational Analysis.

100 In order to identify the relative contributions of each vibrational modes to the overall β-
101 factor, Méheut et al. (2009) developed an approach called "vibrational analysis". In this
102 approach, we consider the β-factor computable from a linear development in $\mu = \frac{1}{m}$:

$$\ln \beta^{44/40} Ca_A \approx \frac{1}{N_q N} \sum_{\boldsymbol{q},i} \left. \frac{\partial \ln(f(\nu^{\mu}_{\boldsymbol{q},i}))}{\partial \mu} \right|_{\mu=\overline{\mu}} \Delta\mu, \tag{3}$$

103 where $\overline{\mu} = (\mu_{44} + \mu_{40})/2$, $\Delta\mu = \mu_{44} - \mu_{40}$ and

$$f(\nu) = \nu \frac{e^{-\frac{h\nu}{2kT}}}{1 - e^{-\frac{h\nu}{kT}}}.$$

104 Eq. (3) expresses the β-factor as a product of the contributions from each vibrational mode.
105 Instead of running over all phonon modes, Eq. (2) can be limited to the Γ-point (q=0)
106 (Dupuis et al., 2015), giving:

$$\beta_{\Gamma}^{44/40} Ca_A = \prod_{i=3}^{3N_{at}} \frac{f(\nu_{44,i})}{f(\nu_{40,i})} \tag{4}$$

107 where $\nu_{44/40,i}$ refers to the frequency associated with the system with all sites occupied by
108 ^{44}Ca or ^{40}Ca isotopes. The product runs over all Transversal Optic modes.
109 By opposition to β_{Γ} , the β-factor defined by Eqs. (1) and (2) will be further referred as
110 "exact".
111 Then, we derive the equivalent of Eq. (3) for Γ-point sampling:

$$\ln \beta_{\Gamma}^{44/40} Ca_A \approx \frac{1}{N} \sum_{i} \left. \frac{\partial \ln(f(\nu^{\mu}_{i}))}{\partial \mu} \right|_{\mu=\overline{\mu}} \Delta\mu = \sum_{i} h_i, \tag{5}$$

112 where we have defined the individual contribution h_i (in ‰) of mode i to the β-factor at Γ.

113 2.3. Error estimation based on experimental frequencies

114 To quantitatively assess the error of our calculated fractionation properties based on existing
115 experimental frequencies, we have set up an original approach. First, the experimental

frequencies are usually only available for limited q-points in the First Brillouin Zone (FBZ), and for the ^{40}Ca material. Except for CaO, they are here originating from IR and Raman spectroscopy, and correspond to the Γ-point (q=0) of the FBZ. For these materials, we have computed the vibrational analysis only at q=0 (Eq. (5)), giving for each frequency its contribution (in ‰) to the β-factor at q=0. Limiting the sampling to the Γ-point (Eq. (4)) shows valid for large systems (Dupuis et al., 2015, for Si isotopes).

In the case of the present study, Table 1 shows the β-factors calculated with the PBEsol functional, exactly (Eqs (1) and (2)) and with Γ-point sampling (Eq (4)). For grossular, $\ln\beta_\Gamma$ shows negligibly different from the exact calculation. For dolomite, calcite, diopside and aragonite, probably due to the small size of some cell parameters, the difference between $\ln\beta$ exact and $\ln\beta_\Gamma$ is not negligible in absolute value (around 1‰). Given the limited relative error, we however expect the Γ sampling as adequate to evaluate the relative contributions of the different parts of the vibrational spectrum to fractionation properties. This is necessary for our correction procedure presented below.

For CaO, since we have dispersion curves giving frequencies on the whole Brillouin zone, and since considering the frequencies at q=0 only gave a result significantly different from the well converged one, we considered the frequencies on a 2x2x2 grid of the Brillouin zone (centered on zero, see Table 1).

For each frequency we can now assess what is its contribution to Ca isotope fractionation properties (h_i) and its offset-vs-experiment (χ_i). To correct for this offset and obtain the "true" β-factor, we will follow the lines exposed in Appendix B of Méheut et al., 2009.

We assume that a calculated frequency $^{40}\nu_i$ *and its corresponding isotopic frequency shift* $^{44/40}\Delta_i = {}^{40}\nu_i - {}^{44}\nu_i$ *are inaccurate by the same relative amount* χ_i*:*

$$^{40}\nu_{i,calc} = \chi_i \times {}^{40}\nu_{i,exp}$$

and

$$^{44/40}\Delta_{i,calc} = \chi_i \times {}^{44/40}\Delta_{i,exp}$$

In this case, this will induce an error $\tilde{\chi_i}$ on h_i equal to:

$$\begin{aligned} \tilde{\chi_i} &\equiv \frac{h_{i,calc}}{h_{i,exp}} \\ &= \chi_i \left(1 + \frac{f^2(u_i) - 1}{1 - f(u_i) cosh(u_i/2)} \right) \end{aligned} \tag{6}$$

with $u_i = \frac{h^{40}\nu_i}{kT}$ and $f(u) = \frac{u}{e^{u/2}-e^{-u/2}}$.

As will be shown below, the frequencies contributing to Ca isotope fractionation at equilibrium extend typically from 150 to 350cm^{-1}. For this range, and for T>300K, equation (6) gives $\tilde{\chi}$ very close to 2χ (more precisely, $\tilde{\chi}$ will be between 1.98χ -for f=150cm^{-1}- and 1.91χ -for f=350cm^{-1}-) . We will therefore consider the following equation to correct the β-factor for frequency errors:

$$\ln \beta^{44/40}_{\Gamma,corr}Ca = \sum_i (h_i \times (1 - 2 * \chi_i)) \tag{7}$$

This equation is strictly equivalent to the following one:

$$\begin{aligned} \ln \beta^{44/40}_{\Gamma,corr}Ca &= (\sum_i h_i) \times (1 - 2 * \overline{\chi}^h) \\ &= \ln \beta_\Gamma \times (1 - 2 * \overline{\chi}^h), \end{aligned} \tag{8}$$

where $\overline{\chi}^h$ is the relative frequency error weighted by the contribution h:

$$\overline{\chi}^h = \frac{\sum_i \chi_i * h_i}{\sum h_i} \tag{9}$$

If this reasoning is correct, the error on the logarithmic β-factors is therefore twice the error $\overline{\chi}^h$. $\overline{\chi}^h$ measures the frequency error *of the frequencies important for Ca isotope fractionation properties*. Practically, $\overline{\chi}^h$ was estimated based on existing experimental data, i.e. the sum in Eq. (9) was realized on the modes for which experimental frequencies are available. The accuracy of this estimate is therefore depending on the completeness of the experimental data.

In addition, if the exact β-factor is different from β_Γ, and if $\overline{\chi}^h$ is known, the same correction can be applied to the exact β-factor:

$$\ln \beta^{44/40}_{corr}Ca = \ln \beta^{44/40}_{exact}Ca \times (1 - 2 * \overline{\chi}^h) \tag{10}$$

In the literature (e.g. Schauble et al., 2006), the correction for functional error on vibrational frequencies is realized through a "scaling factor" (SF), equivalent to multiplying all frequencies by the same $\overline{\chi}$ factor, that we will determine here by directly averaging the χ_i:

$$\ln \beta^{44/40}_{corr-SF}Ca = \ln \beta^{44/40}_{exact} \times (1 - 2 * \overline{\chi}) \tag{11}$$

with:

$$\overline{\chi} = \frac{\sum_i \chi_i}{nfreq} \tag{12}$$

with $nfreq$ the number of available experimental frequencies.

2.4. DFT calculations

The phonon frequencies are computed from first principles using density functional theory (DFT) (Hohenberg and Kohn, 1964; Kohn and Sham, 1965).

The core approximation that permits electronic structure calculations based on DFT resides in the building of an approximate functional that describes the relation between the electronic density and electronic energy.

The choice of the functional can be rooted on various considerations. The simple local density approximation (LDA), such as parametrized by Perdew and Zünger (PZ, Perdew and Zunger, 1981), is numerically very efficient. It has been shown reliable for silicate systems to predict their structural, vibrational and thermodynamical properties such as state diagrams (e.g. Tsuchiya et al., 2004). It was chosen by Fang Huang et al. to compute Ca isotope fractionation in anhydrous silicates and carbonates (Wang et al., 2017b; Huang et al., 2019). The PZ functional is however inadequate for materials containing hydrogen. Gradient-corrected functionals such as PBE (Perdew et al., 1996); BLYP (Becke, 1988; Lee et al., 1988) are prefered in this case. These functionals were used in our preceeding works on Si, O and H fractionation properties (Méheut et al., 2010, 2014; Füger et al., 2018). On the other hand, Rustad et al., 2010, Colla et al., 2013, and Moynier and Fujii, 2017 focus on the more evolved B3LYP functional (Becke, 1993). Several properties of the Ca atom appear to be very sensitive to the choice of the functional, but so far little is known about their reliability. An illustrative example of this is the number of water molecules in the coordination sphere of the Ca^{2+} aquo ion as inferred from molecular dynamics simulations, that vary from 5 to 10 depending on the way the atomic interactions are taken into account (considering both electronic structure and calculations based on empirical potentials, Chizhik et al., 2016). Experimental results (X-ray, Neutron Diffraction or EXAFS studies) are, in this regard, no more conclusive (see discussion in Chizhik et al., 2016). Considering only methods based on first-principles calculations, the range of coordinations found for $Ca^{2+}_{(aq.)}$ is smaller (6-7, Baer and Mundy, 2016 and references therein), but their reliability remains

questioned, and a limited number of functionals have been tested so far (BLYP, PBE, HCTH, PBE96, Chizhik et al., 2016). Baer and Mundy (2016) argued on the validity of a calculation based on the BLYP functional in addition to the dispersion correction (D2) put forth by Grimme (Grimme, 2004). This correction, intended to remedy to the incomplete account of weak dispersion forces by gradient-corrected functionals, is generally considered for aqueous systems. Theoretical schemes accounting for dispersion forces (vdW-DF2 functional, Lee et al., 2010) were tested to compute Si fractionation properties (Stamm et al., 2020), but did not show any net advantage in that particular case. As illustrated above, the choice of the functional is generally system dependent. However, as fractionation properties result from the thermodynamic equilibrium between various phases, it is utterly important to find a theoretical scheme that is able to properly model various kinds of systems with the same level of accuracy. As such, the efficiency of our theoretical scheme is primarily estimated as its consistency, i.e. its capacity to induce errors that are as much system-independent as possible.

In this work we have used the local approximation of Perdew and Zunger (PZ) (Perdew and Zunger, 1981), the generalized-gradient approximations to the exchange-correlation functional of Perdew, Burke and Ernzerhof (PBE) (Perdew et al., 1996) and of Becke, Lee and Par (BLYP) (Becke, 1988,Lee et al., 1988). We have also considered calculations with the vdW-DF2 non-local functional (Lee et al., 2010), and calculations with the BLYP functional with the Grimme-D2 correction (BLYP-GD2) (Grimme, 2006,Barone et al., 2009). Those two theoretical frameworks are considered here for their interest to treat aqueous systems (Baer and Mundy, 2016, Ducher et al., 2017), as the fractionation properties of aqueous Ca are of high interest for Ca isotopes geochemistry. Here, the materials in consideration should not require such theoretical frameworks. However, as isotopic fractionation is measured between two different phases, it is of primary importance to treat both systems consistently, to avoid systematic errors. As a consequence, if the treatment of Ca in solution requires the use of BLYP-GD2 or vdW-DF2 frameworks, it is essential to check for their efficiency for crystalline solids as well. A last functional, PBEsol (Perdew et al., 2008) was also tested here. This functional previously showed efficient as an alternative to B3LYP in the challenging case of the aragonite-calcite equilibrium (Demichelis et al., 2017).

Ionic cores of each atom are described by norm-conserving pseudopotentials (Troullier and Martins, 1991) in the Kleinman-Bylander form (Kleinman and Bylander, 1982). The pseu-

dopotentials used for Al, Si and O are described in the electronic annexes of Méheut et al. (2007). The pseudopotential used for C is described in Füger et al. (2018) . The pseudopotentials used for Ca and Mg were taken from the PSlibrary (Dal Corso, 2014).

Computational details for calcite are the same as in Füger et al. (2018) . For all other minerals (lime CaO, dolomite, aragonite, diopside, grossular), the electronic wave-functions are expanded in plane-waves up to an energy cut-off ϵ_{cut} =80Ry, and the charge density cut-off is $4\epsilon_{cut}$.

The electronic integration is performed by sampling the Brillouin zone with a 4×4×4 k-points grid for CaO, a 3×3×3 k-point grid for dolomite, a 3×2×3 k-points grid for aragonite, and a 2×3×2 k-points grid for diopside according to the Monkhorst-Pack scheme (Monkhorst and Pack, 1976). Due to the large unit-cell of grossular, the electronic sampling can be restricted to a single k-point (1/4, 1/4, 1/4), chosen according to Baldereschi (1973).

Phonon frequencies are computed using linear response theory (Baroni et al., 2001), with the Quantum-Espresso package (Giannozzi et al., 2009). Interatomic force-constants are obtained from the dynamical matrices computed exactly (within DFT) on a $n \times m \times p$ grid of q-vectors (4×4×4, 2×3×2, 3×2×3 and 1×1×1 for CaO, diopside, aragonite and grossular, respectively)

Long-range effects are taken into account by computing Born effective-charges and static dielectric constants (Baroni et al., 2001). Dynamical matrices and thus phonon frequencies, can then be obtained in any point of the reciprocal space by Fourier-interpolation of the force constants. For all materials, the vibrational partition function (Eq. (2)) is converged with a 5×5×5 interpolation grid.

3. RESULTS

3.1. Structural properties

The relaxed structures are reported in Table EA-1, for each material and within each of the 6 theoretical schemes considered here. Average Ca-O distances are also reported. Since those distances are often correlated with equilibrium fractionation properties, an efficient way to comment on the efficiency of the various theoretical schemes is to look a their error on average Ca-O distances. On Figure 1, we report the relative error of each calculations

on average Ca-O distances $< Ca - O >$.

It shows that the PZ functional tends to underestimate CaO distances (and cell parameters, cf Table EA-1), whereas PBE and BLYP functionals tend to overestimate them, consistently with previous studies (for PZ functional: see e.g. Huang et al., 2019; for PBE and BLYP functionals: see e.g. Méheut and Schauble, 2014, Dupuis et al., 2015). The vdW-DF2 and BLYP+GD2 calculations, that have been implemented to effectively correct for the shortcomings of GGA functionals in accounting for the weak Van der Waals forces (Kristyán and Pulay, 1994), show contrasting results. Adding the Grimme-D2 correction to the BLYP functional (BLYP+GD2 scheme) leads to smaller (and closer to experiment) structural parameters, which seems reasonable considering that the Grimme-D2 correction corresponds to adding an attractive force. On the contrary, calculations with the vdW-DF2 functional lead to elongate Ca-O distances ($+1.7\pm0.3\%$) and cell parameters, in particular relative to PBE ($+1.0\pm0.4\%$ for $< Ca - O >$). This is contradictory with our results in Stamm et al., 2020, which were dealing with organic materials containing Si-O bonds. In that case, the vdW-DF2 lead to cell parameters smaller than PBE, and closer to experiment, whereas Si-O bond lengths were the same with PBE and vdW-DF2, as expected (Supplemental Table A.1 of Stamm et al., 2020). For the materials considered in this study, the improvement of vdW-DF2 over PBE is not clear. Lastly, in terms of the general agreement with experiment, the PBEsol calculation shows the best result, with a difference of $-0.45 \pm 0.25\%$ relative to measured bond lengths.

In terms of the overall variation of the error of a given theoretical scheme from one material to the other (hereafter called spread), the PBEsol calculation shows also superior to the others (except vdW-DF2, cf Table EA-1), with a spread of 0.25%, versus 0.4% to 0.7% for the other calculations. It means that, as fas as we can judge, PBEsol (together with vdW-DF2) is more consistent, or more transferable than the other theoretical schemes.

Lastly, it should be noted that the structural parameters of CaO, calcite, dolomite and aragonite are usually more underestimated (or less overestimated), whereas the structural parameters of grossular and diopside are generally less underestimated (or more overestimated). There is however no systematic trend.

3.2. Vibrational properties

Tables EA-2 to EA-7 present, for each material considered here and the 6 considered theoretical schemes (functionals+correction), the complete vibrational properties, and compare them with experimental frequencies. For the frequencies that could be compared to their measured counterpart, we computed the offset $\chi_i = \frac{\nu_{th}}{\nu_{exp}}$.

Figure 2, corresponding to our PBEsol calculation, shows typical patterns for the $\chi(\nu_{exp})$ diagram: for CaO, calcite and aragonite, χ is highly variable below 400 cm^{-1}, and much less for higher frequencies. In comparison, the two silicates grossular and diopside show much less scatter below 400 cm^{-1}. Note that, as discussed in 3.3, the 0-400cm^{-1} interval is associated with the largest contribution to Ca isotope fractionation properties at equilibrium.

This can be seen also based on statistical analysis (see Fig.3). For the PBEsol functional, the variability of χ ($\sigma(\chi)$) is 3.7%, 3.6% and 4.0% for CaO, calcite and aragonite, respectively, and only 1.3% and 1.7% for grossular and diopside, respectively.

Note also that for aragonite with the BLYP functional (with or without Grimme-D2 correction), two calculated frequencies are negative ($B_{2u}(1)$ and $A_u(1)$, Table EA-5). Although this may appear as an argument to disqualify this functional, those frequencies contribute negligibly to the β-factor (see discussion below), so we decided to simply exclude them from our estimations.

Based on statistical analysis, Fig.3 shows that, for a given material, the variability of the frequency error χ ($\sigma(\chi)$) can be quite important, up to 12.3% for the BLYP calculation of calcite. Not surprisingly, this variability is generally smaller for the two silicates considered here, as underlined above for PBEsol. Noticeably, PBEsol shows the lowermost variability $\sigma(\chi)$ compared to other theoretical schemes for all materials, with a few cases where PZ or PBE show equivalent results. Interestingly, even B3LYP calculations found in the literature do not show less variability than PBEsol. Looking at the spread (total domain of variation of $\overline{\chi}$ between the different materials), PBEsol shows also more consistent than other schemes except PZ. However, to conclude on the consistency of a given theoretical scheme, it is better to take into account the contribution of the various frequencies to the fractionation, as Ca fractionation is related to some particular modes only. This will be discussed below.

3.3. β-factors and correction

The results will be discussed in terms of the logarithmic β-factors ($\ln\beta$) and logarithmic fractionation factors ($\ln\alpha$) expressed in parts per thousand (‰). Table 2 summarizes all the fractionation properties calculated at 300K within all the theoretical frameworks considered. Figure 4 represents all the mineral pair fractionations calculated here.

Tables EA-2 to EA-7 present, for each material considered here and the 6 considered theoretical schemes (functionals+correction), the complete vibrational properties at the Γ-point, the calculated exact logarithmic β-factors at 300K, and the contribution h_i of each Γ-point vibrational frequency to the β-factor (except for CaO, for which a 2x2x2 Brillouin Zone Sampling is considered).

Fig 5 visualizes these contributions h as a function of theoretical frequencies, and their integrated value (for the PBEsol calculations only, since thhe general features of these curves do not depend on the theoretical scheme). The main contributing frequencies are in the range 100-400cm^{-1}. Note, however, that the silicates (grossular and diopside) show high-frequency contributions, if not dominating, at least much higher than for the other materials, in particular the carbonates. Those high vibrational frequencies correspond to modes (i.e., collective atomic displacements) implying the displacements of the more strongly bonded atoms (SiO, AlO). The fact that they are contributing to the fractionation of Ca isotopes means that the Ca atom is in fact displaced in those modes, even if slightly. In other words, the Ca atom appears dragged by the high-frequency displacement of other structural units (in particular, SiO_4 or AlO_6), resulting in a contribution of those high-frequency modes to fractionation.

Lastly, Tables EA-2 to EA-7 also compare calculated and experimental frequencies, giving the offset χ_i and the corrected β-factor at 300K following Eqs. (11) or (9). Table 2 summarize these fractionation properties (raw and corrected) at 300K.

4. DISCUSSION

4.1. Uncertainty on Ca fractionation

As seen on Figure 4, the calculated fractionation properties are varying significantly, typically by 1‰, between the different theoretical frameworks. More precisely, the variation due

to the theoretical framework, hereafter called "functional spread" goes from 0.4‰ for the grossular-aragonite pair (fractionation between 7.3 ‰ for BLYP and 6.9 ‰ for vdW-DF2) to 1.7 ‰ for the grossular-diopside pair (fractionation between 4.5 ‰ for PZ and 2.8 ‰ for BLYP+D2). Trying to acknowledge if some minerals are more problematic than others, one can observe that diopside appears the most (three times over four) in pairs showing the largest functional spreads. Mineral pairs involving only carbonates show on average less functional spread (from 0.5 to 0.9), but this is clearly not the case among silicates, as exemplified by the grossular-diopside pair. In any case, this variation due to theoretical framework appears significant with respect to the corresponding fractionations, and well above the level of analytical accuracy of isotopic measurements.

Trying to acknowledge which functionals behave worse, we can observe that PZ, and functionals accounting for van der Walls interactions (BLYP+D2, vdW-DF2) behave particularly badly. Indeed, from our 15 mineral pair calculations, we have 30 "extreme" calculations (i.e. theoretical schemes representing either the larger or the smaller value for a given fractionation). These extreme values are coming from BLYP-D2 (10 times), PZ (7 times), vdW-DF2 (6 times), PBEsol (4 times), BLYP (2 times) and PBE (once).

4.2. Correction procedure

The interest of the above discussion is that it is independent of any correction. Its weakness is that we don't know what the correct fractionation could be, in order to determine which functional may approximate it best.

To improve the accuracy of those calculations, several works (e.g. Schauble et al., 2006, Méheut et al., 2009) have attempted to correct for the error on frequencies, based on experiment.

4.2.1. Scaling factor

The common approach assumes that a given theoretical scheme systematically underestimates or overestimates all vibrational frequencies by the same relative amount. Likewise, the average relative error on frequencies ($\overline{\chi}$, Eq. (12)) is computed. $\overline{\chi}$ is then used to correct all frequencies, leading to Eq. (11) for the β-factor.

If the starting hypothesis was correct, this procedure should give the same result for any functional, as it corrects for its systematic error. Figure 6 illustrates this procedure for the β-factors of calcite. The black filled symbols represent the β-factors computed within the different theoretical frameworks. Then, from the comparison of the calculated vibrational properties with experiment, an average scaling factor is obtained ($\overline{\chi}$), for each theoretical scheme (for calcite, $\overline{\chi}$=+2.1%, -8.2%, , -6.3%, -9.1%, -7.3% and -3.4% respectively for PZ, PBE, vdW-DF2, BLYP+D2, and PBEsol, cf Table EA-3). This unique factor is then used to correct fractionation properties (Eq. (12), blue empty symbols on Figure 6). The outcome of this approach is disappointing: indeed, the corrected β-factors show the same dispersion as the raw ones, before correction.

Table 1 further illustrates the functional spread on β-factors for each mineral, before (first line for each mineral) and after rescaling (second line). In general, the rescaling procedure indeed reduces the spread, but with very variable efficiencies (almost nul for calcite - see Figure 6 - for which the spread goes from 3.6 to 3‰, to quite high for CaO, for which the spread goes from 3.11 to 0.59). However, when mineral pair fractionations are now considered instead (lower part of Table 1), the spread always increases upon rescaling. This means that rescaling increases the uncertainty of calculated fractionations, instead of decreasing it.

It stems from the high variability of the frequency error χ, and from the very different contribution of each modes to Ca fractionation properties. Figure 2 shows typical plots of the error as a function of the frequency for different materials, for PBEsol calculations. The frequencies more important for Ca fractionation properties are essentially below $400cm^{-1}$ (see Fig 5 and section 3.3). Their relative error with respect to experiment χ_i is highly variable from one material to the other. χ_i is also varying a lot between different modes, particularly for calcite, CaO and aragonite. Statistically speaking, the average rescaling factor presents a high uncertainty, as shown on Figure 3. For example, for the PBE calculation we have $\chi = -2.0 \pm 8.2\%$ for calcite, and $\chi = -8.2 \pm 8.8\%$ for aragonite. Correcting uniformly for these errors without further caution (e.g. for PBE, taking scaling factors of 1.02 for calcite and 1.082 for aragonite) leads to fractionations even more variable from one theoretical framework to the other, than without correction.

4.2.2. Improved procedure

To correct for theoretical errors on fractionation properties based on experiment, it is necessary to account for the relative contributions of each frequencies. The most important modes are those for which the Ca atom will move the most, as it is the condition for the Ca mass to affect the frequency. These important modes can be identified based on vibrational analysis. Fig. 5 shows vibrational analyses for the materials considered here. The important frequencies are concentrated in a narrow range of low frequencies, typically between 150 and 350cm^{-1}. Note that this frequency range corresponds also to largest uncertainties on χ (Figure 2).

The procedure consists in calculating a "h-weighed" scaling factor $\overline{\chi}^h$ (Eq. (9), see section 2.3), h denoting the contribution of a particular mode to $\ln\beta$ (Eq. (5)) . Table 2 and Figure 7 present the results of this procedure, (see also Figure 6 illustrating the particular case of calcite). On the β-factors, this improved correction significantly reduces the functional spread, typically around 0.5‰, with larger values remaining for grossular and dolomite ($\approx$ 1‰).

For the calculated fractionation factors relative to calcite, shown on Table 2 (and Fig. 8), it also permits an improvement of the spread by a factor of approx. 2 except for grossular-calcite and dolomite-calcite pairs.

A worse spread after correction could be due to an incomplete (and not representative) sampling of the vibrational properties of a mineral by experiment. This is particularly expected for grossular. Indeed, among the 97 different vibrational frequencies of grossular corresponding to Γ-point modes, 55 are silent (meaning that they are neither IR nor Raman-active), and therefore impossible to sample experimentally (except possibly by neutron inelastic scattering). Four other modes could not be associated with an experimental frequency, possibly due to insufficient spectroscopic intensity. In total, these 59 "orphan" modes contribute for more than 50% of the β-factor ($\sum_{orphan} h$ in Table EA-6). The estimate of $\overline{\chi}^h$ for grossular, that is based upon existing experiment, might therefore be less accurate than for minerals with a more complete set of active vibrational frequencies. Other important orphan contributions are for calcite (25% of the total), whereas it is $\approx$ 10% for aragonite and diopside. CaO lime and dolomite show no orphan contribution, and are therefore the better determined minerals. They should be preferentially used as reference for fractionation in mineral pairs.

On Table 3, we represent the functional spread before and after correction for each of the 15 independent mineral pairs. We can observe that (i) correction generally reduces the spread, except for calcite-dolomite, grossular-calcite, grossular-aragonite and CaO-diopside. (ii) the pairs not implying grossular or calcite show generally lower spreads after correction (the worse being 0.8‰ for dolomite-diopside), whereas the presence of grossular or calcite among the pair tends to increase the spread after correction.

Overall, if the improvement with the standard rescaling procedure is real, the improved procedure does not significantly reduce the functional variability. It does not permit to attain uncertainty ranges comparable to analytical uncertainty. Keeping only mineral pairs involving CaO, aragonite, diopside and dolomite (green and black pairs on Table 3), we obtain spreads of 0.3 to 0.8‰ after correction, which could be taken as representative of the uncertainty attached to our correction procedure.

Other origins for this variability after correction could be errors on experimental frequencies, anharmonicity (unaccounted for by theory, implicitly present in experimental frequencies), or the difference between the displacements of the calculated modes and the real ones. In fact, looking at the contributions (h values) of similar modes in different calculations of the same material (important modes are emphasized in bold character in Tables EA-2 to EA-7), we can see that similar modes contribute very differently. For example, for dolomite (Table EA-4), the $A_u(2)$ mode contributes for 0.62 ‰ when calculated with BLYP, but for 0‰ when calculated with PZ. It means that the mode that is assimilated to the same displacement, associated with the experimental frequency at 361 cm^{-1}, in fact implies the displacement of the Ca atom with BLYP, but not with PZ. This likely reflects some complex effects related to diagonalization of slightly different matrices holding significantly different eigenvectors with similar eigenvalues, and puts some limits to a proper comparison with experiment.

In the following, this correction procedure will be further used to determine the efficiency of the different functionals. Efficient functionals should give similar results whether corrected or not.

4.3. Evaluation of the different functionals

Ideally, the efficiency of a functional should be estimated towards the exact isotope fractionation values (α-factors between two minerals). We do not know of accurate and reliable

estimates of Ca isotope mineral-pair equilibrium fractionation. However, our corrected isotope fractionation properties may serve as estimates for those exact values. On Figure 9, we chose to estimate the error of a scheme by the difference between the raw and corrected isotope fractionation properties for this scheme. An efficient functional should change little with correction.

Figure 9 demonstrates the general superiority of the PBEsol functional in that matter (PBE being almost as effective). Its estimated error remains below 0.67‰ for all mineral pairs not including grossular (for which the correction is very uncertain, see 4.2.2), whereas all other schemes except PBE present errors larger than 1 ‰ in some cases. We have also considered the functional spread after correction (Table 3) as an estimate of the uncertainty of our procedure (dashed line on Figure 9). As seen on Figure 9, the error estimated for PBEsol remains below the inferred procedure uncertainty, except for grossular-dolomite and CaO-dolomite isotope fractionations (for which PBEsol presents the smaller estimated error).

In a different attempt to characterize the error of a theoretical scheme, we considered the difference of a raw calculation with the average isotope fractionation value after correction (=average of the corrected isotope fractionation for a given mineral pair over the different theoretical schemes), as it could be considered a better estimate of the "exact" value. This alternative estimate of the error do not show very significantly different than the former one. Our first approach therefore appears satisfactory to estimate the efficiency of a functional. In this approach, following Eq. (8), $2\overline{\chi}^h$ appears naturally as an estimator of the relative error of our procedure on the $\ln\beta$ values (in %). For this error to cancel out on isotope fractionation factors, it should be independent on the mineral. In this regard, the better accuracy of PBEsol is a consequence of its higher consistency on errors of vibrational frequencies, as visualized on Figure 3.

Note also that, as discussed in the results section, the PBEsol functional showed superior to the other frameworks regarding (1) the absolute accuracy on structural parameters and average Ca-O distances in particular (Figure 1); (2) the amplitude of the spread on structural parameters, depending on the material (Figure 1); (3) the total χ variability for the frequencies of a given material ($\sigma(\chi)$, Figure 3). Considering that our correction procedure is only possible when experimental frequencies are available and exhaustive, which is far from systematic, and that our correction appears to present some uncertainty (around 0.8‰, see 4.2.2), we argue that the PBEsol functional gives the most reliable results without

correction, at least for materials comparable to those present in this study.
In the same order of idea, the estimated error for the PBEsol functional (red squares on Fig9) is essentially comparable to the assessed uncertainty of this error estimation (dashed line on Fig9).
Following these remarks, we recommend the raw PBEsol calculations as most reliable for estimating isotope fractionation properties. Our recommended isotope fractionation laws are listed in Table 4 .

4.4. Comparison with previous calculations

Previous works (Rustad et al., 2010; Wang et al., 2017a; Wang et al., 2017b; Antonelli et al., 2019; Huang et al., 2019) have estimated Ca isotope fractionation properties between the same mineral pairs considered here. Table 5 compares the fractionations obtained by these authors for the dolomite-calcite, aragonite-calcite, grossular-diopside and grossular-lime mineral pairs.
Our results show a fair agreement with Antonelli et al. (2019), and with the aragonite-calcite and dolomite-calcite calculations by Wang et al. (2017b), but our results significantly differ from Rustad et al. (2010) for dolomite-calcite (-0.9‰ vs -2.3‰), and with Huang et al. (2019) for grossular-diopside (4.2‰ vs 5.8‰). Our calculations differ from these authors by the choice of functional: Rustad et al. (2010) used B3LYP, whereas Huang et al. (2019) uses PZ. To evaluate the role of the functional in these discrepancies, we compare in Table 5 calculations realized with the same functionals.
Regarding Rustad et al. (2010), unfortunately, we cannot use B3LYP in our theoretical framework. Instead, we computed the calcite β-factor with the BP86 functional, that can be compared with their work (Table 5). Whereas their BP86 $\beta_{calcite}$ calculation is very similar to their reference B3LYP one (16.01‰ vs 16.18‰), our BP86 calculation yields a much lower value (12.26‰), similar to our PBE result (12.05‰). This suggests that other details of Rustad et al. (2010) calculations may have significant effects on the final result. These calculations differ from ours by two aspects: first, Rustad et al. (2010) use gaussian basis sets for electronic wave-function description, and second, they use cluster-like models when we use periodic boundary conditions. Rustad et al. (2010) did not see any significant effect of the choice of gaussian basis set (6-31G* vs 6-311++G(2d,2p) on the mineral β-

factors. On another hand, based on a periodic boundary calculation with Gaussian basis sets, Valenzano et al., 2007 and De La Pierre et al., 2016 report different values for the Eu(2)TO frequency determined experimentally at 223 cm^{-1} : respectively 219.6 [-1.5%] and 225.2 [+1.0%]. In terms of its contribution to isotope fractionation, this makes a 5% difference, still far from the 25% observed between our BP86 calculations of calcite and the one of Rustad et al. (2010). Further investigations will be necessary to clarify this matter. Regarding the works of Fang Huang & al. (Wang et al., 2017a, Wang et al., 2017b and Huang et al., 2019), excluding the role of the functional is quite straightforward, since we realized PZ calculations. The comparison (Table 5) shows the β-factors that we calculate with the same functional to be systematically lower than theirs, by various amounts, from 0.5-0.8 ‰ at 300K for calcite, dolomite, diopside, aragonite (by order of increasing difference), and up to 1.75 ‰ for grossular. As for the works of Rustad & co-workers, the functional cannot be claimed as the sole parameter responsible for the differences between the two calculations. To further document the discrepancies between both studies, we compared the relaxed structural parameters on Table 6. On the whole, our calculated cell parameters and Ca-O distances are lower (by ≈1%) than Fang Huang & al's. We looked at other studies using periodic boundary conditions, plane-wave basis sets and pseudopotentials (or, for CaO, all-electron calculations) and the PZ functional. For CaO lime, calcite, dolomite and aragonite, we found several works fairly consistent with our findings. We hypothesize that the discrepancies of Fang Huang & al originate from inequivalences posed by using different pseudopotentials and other convergence parameters.

4.5. Comparison to isotope fractionations measured in experiment and Nature

The Ca isotope fractionation factor between calcite and fluid is the most well studied example. For this mineral-fluid pair however, an unambiguous isotope fractionation factor under isotopic equilibrium conditions does not exist. At present the general consensus is that no isotope fractionation occurs between calcite and the forming fluid. This argument is based on the observations by Fantle and DePaolo (2007) that no difference occurs between carbonitic nannofossil ooze and chalk and pore fluid samples from ODP Site 807A in Ontong Java Plateau. This negligible isotope fractionation between solution and calcite at low precipitation rates was further confirmed by aquifer studies (Jacobson and Holm-

den, 2008). Note however that this value has not been confirmed to date from experimental studies. To model the dependence in growth rate of experimentally defined Ca isotope fractionation between nucleated calcite and fluid, DePaolo (2011) suggest that slightly larger values ($\Delta^{44/40}\mathrm{Ca}^{eq}_{calcite-fluid}$ = -0.5 to -0.2‰) should be considered at equilibrium. More recently Oelkers et al. (2019) studied isotopic fractionation between calcite and Ca (aq) at near equilibrium conditions using a pH-jump technique, where calcite initially dissolved at pH 6.2 and precipitated at pH 7.5. They reported calcite fluid isotope fractionation factors at equilibrium of -0.8‰ for the precipitation phase and -1.6‰ for the dissolution phase of the experimental runs, arguing that the difference likely stems from the speciation of Ca in the fluid phase, which exhibits differences due to the prevailing pH. As we did not compute a dissolved Ca β-factor, we cannot compare our calculations directly to mineral-fluid experiments. In the following, to compare our calculated $\Delta^{44/40}\mathrm{Ca}^{eq}_{mineral-calcite}$ with existing $\Delta^{44/40}\mathrm{Ca}^{eq}_{mineral-fluid}$, we will combine them to obtain the value of $\Delta^{44/40}\mathrm{Ca}^{eq}_{calcite-fluid}$ that would be consistent if all values were representing equilibrium, and discuss this value.

For the dolomite-calcite isotope fractionation, Holmden (2009) report a difference in $\delta^{44/40}Ca$ of -0.61‰ between dolomite and calcite in natural systems (sediments). This value compares well with our estimated -0.9‰ estimate of the dolomite-calcite isotope fractionation at 300K, and even more if we consider that the equilibration temperature might be larger ($\Delta^{44/40}\mathrm{Ca}^{eq}_{dolomite-calcite}$ = -0.5‰ at 125°C, see below). Note however that Holmden (2009) considered as a starting hypothesis that the dolomite-calcite Ca isotope fractionation should be null at equilibrium ($\Delta^{44/40}\mathrm{Ca}^{eq}_{dolomite-calcite}$ = 0). They chose to interpret their results as a consequence of the isotopic signature of the involved reacting fluids.

For the dolomite-fluid system, experimental works under hydrothermal conditions (125°C) report a $\Delta^{44/40}\mathrm{Ca}_{dolomite-fluid}$ = -1.2‰ during dissolution, under conditions interpreted as close to equilibrium (Perez-Fernandez et al., 2017). At the same temperature, we find $\Delta^{44/40}\mathrm{Ca}^{eq}_{dolomite-calcite}$ = -0.5‰. Our calculation and Perez-Fernandez et al.'s study would be consistent for $\Delta^{44/40}\mathrm{Ca}^{eq}_{calcite-fluid}$ = -0.7‰ at 125°C. Considering that $\Delta^{44/40}\mathrm{Ca}^{eq}$ values are essentially proportional to $\frac{1}{T^2}$, they should be twice as large at 300K compared to 125°C ($\frac{400^2}{300^2}$=1.8). This would translate into $\Delta^{44/40}\mathrm{Ca}^{eq}_{calcite-fluid}$ = -1.3‰ at 300K. This value seems incompatible with the general consensus ($\Delta^{44/40}\mathrm{Ca}^{eq}_{calcite-fluid}$ = 0‰), suggesting that Perez-Fernandez et al's experiments might not be fully equilibrated. Only the larger estimate of Oelkers et al. (2019) ($\Delta^{44/40}\mathrm{Ca}^{eq}_{calcite-fluid}$ = -1.6‰) would be consistent.

For the aragonite-fluid system mineral growth experiments at low degrees of saturation of the fluid do not exist in the literature. Both the experimental works by Gussone et al. (2003) and AlKhatib and Eisenhauer (2017) exhibit $\Gamma_{aragonite}$ values >25. In both these studies however aragonite is enriched in the lighter ^{40}Ca isotope, by approximately -1.7‰ at the lower precipitation rates, closest to equilibrium. At the same temperature, we calculate: $\Delta^{44/40}\mathrm{Ca}^{eq}_{aragonite-calcite} = -3‰$, therefore $\Delta^{44/40}\mathrm{Ca}^{eq}_{calcite-fluid} = -1.3‰$ would be necessary to reconcile our calculations with those estimates. This is surprisingly similar to what we find based on dolomite-fluid estimates of Perez-Fernandez et al. (2017), and suggests again that those experiments might not be fully equilibrated.

4.6. Controlling parameters of Ca isotope fractionation: anionic group dragging

In Table 7, we compare the calculated β-factors with various structural properties. The two parameters that have been the most discussed in the literature are coordination (e.g. Colla et al., 2013) and CaO distances (e.g. Huang et al., 2019). Figure 10 reports our calculated isotope fractionation properties as a function of Ca-O distance.

A particularly striking feature of our results is the very high β-factor of grossular, although Ca in this mineral presents a VIII coordination (versus VI for CaO, calcite, dolomite), and its Ca-O distance is longer than in calcite, and similar to that in CaO. The vibrational analysis (reported in Fig.5) shows that for the silicates grossular and diopside, the contributions of high frequencies, although not the main ones, are not negligible, and "make the difference" with e.g. carbonates, for which the highest frequencies contributing are around 300cm^{-1}. Those high-frequency modes are mainly modes implying Si-O or Al-O bonds, and the contribution of those modes to Ca isotope fractionation means that those modes "drag" the Ca atom. This coupling, or this interference of the Ca atom with those high frequency atomic displacements, seems able to explain that the β-factor of grossular is finally larger than carbonates, when all frequencies have been considered. On the contrary, carbonates do not show this high-frequency contribution, as the CO stretching modes appear uncoupled with the Ca displacements. Such a control of strong anionic groups on the isotopic fractionation of cations has already been proposed to account for Zr isotope fractionation in minerals (Méheut et al., 2021). The question that remains to answer is why some modes are coupled whereas some others are not.

Apart from this control of strong anionic groups coupled to the atom of interest, it cannot be excluded that Ca-O distance is correlated with Ca isotope fractionation properties, for similar materials at least. On Figure 10, we show in particular that the isotope fractionation properties of silicates (diopside, grossular) and carbonates (at least dolomite and calcite) evolve on straight lines of similar slopes, as a function of Ca-O distances. Aragonite, however, does not follow the trend of dolomite and calcite, suggesting that coordination might also influence this relationship. On another hand, CaO lime, which presents a perfectly regular CaO octahedron, is much heavier than calcite and dolomite, of the same coordination but much more distorted. In this case, it is tempting to invoke a potential control of polyhedral distortion.

Although practical to predict isotope fractionation properties, the correlation with CaO distances asks for tangible explanations. In the case of dolomite versus calcite, one has to recognize that other parameters, such as those measuring polyhedral distortion, do not make sense: dolomite is less distorted than calcite but shows shorter CaO distances whereas we would have expected CaO distances to decrease with decreasing distortion, not increase. In those conditions, and in line with our study on the structural controls of Si isotope fractionation (Méheut and Schauble, 2014), it is tempting here to invoke the different electronegativity of Ca versus Mg to explain the increasing CaO bond-length - and decreasing isotope fractionation properties - of dolomite versus calcite.

5. CONCLUSION

- In this work, we have estimated Ca isotope fractionation properties between carbonate, silicate and oxide minerals presenting accurate experimental estimates of their vibrational frequencies. Six theoretical frameworks were considered, showing results varying from single to double.

- To evaluate the efficiency of those theoretical frameworks, we tried to correct our calculated isotope fractionations, accounting for the error shown between calculated and experimental frequencies. The classical approach, assuming an identical error for all frequencies, appeared quite disappointing, in that corrected isotope fractionations did not show less variable than raw ones. We have set up an original approach for a more accurate correction. It relies on the estimate of the contribution of individual frequen-

cies to isotope fractionation properties. To be efficient, it requires to have exhaustive experimental estimates for the modes contributing the most to isotope fractionation properties. The case of grossular, for which more than half of the contributive modes are silent, is most illustrative.

- At the term of this correction, PBEsol and PBE functionals appear the most efficient, BLYP and BLYP+GD2 being approximately equivalent, and PZ and vdW-DF2 being significantly worse. From the point of view of several other criteria, PBEsol appears superior for the considered materials: (1) the consistency of the frequency error χ_i for different modes of a given material, (2) the consistency of the average frequency error $\overline{\chi}$, or of the average error weighted by the contribution to the β-factor $\overline{\chi}^h$ for different minerals, (3) the amplitude of this average frequency error (4) the amplitude and consistency of the error on average CaO distances. Said differently, not only PBEsol gives better results (closer to experiment) for these properties, but it also gives results with a more systematic error with respect to experiment. For these reasons, we judge this theoretical scheme as the most reliable to predict the fractionation of Ca isotopes at equilibrium.

- The comparison with other estimates in the literature reveals the crucial importance of all numerical aspects of those calculations, such as electronic basis sets, or modelling approach (periodic boundary versus cluster modelling).

- This sensitivity to numerical details may seem specific to Ca isotopes. In fact, for Si or O for example, calculated properties appeared influenced only slightly by the considered numerical schemes (Méheut et al., 2007: PZ vs PBE for oxygen isotopes; Dupuis et al., 2015: BLYP vs PBE for Si isotopes , Stamm et al., 2020: vdW-DF2 vs PBE for Si isotopes). However, Si^{4+} is a strong cation, and its bonds are changing only marginally with distortion. On another hand, Ca^{2+} is a weak cation, which environment is easily influenced by its environment and the volume/hindrance if its neighbours. It is therefore not completely surprising that its vibrational and fractionation properties are different for schemes (PZ vs PBE for example) for which Si-O bonds are significantly different. This sensitivity might be found for other weak cations, such as K, Ba, or Sr for example.

- In the systems considered, and independently of CaO bond lengths, the fractionation of Ca isotopes appears strongly affected by anionic group dragging, i.e. the presence of strong anionic groups (such as SiO_4 or AlO_6 groups in silicates) vibrating at high frequency *and* which atomic displacements are "dragging" the Ca atom. This was previously observed for predicted Zr isotope fractionation properties (Méheut et al., 2021).

Acknowledgments

This research was founded by l'Agence Nationale de la Recherche (ANR) through grant FILi-CaBeSo ANR-19-CE01-0016 (Fractionation of Isotopes in Liquids - Calcium Behaviour in Soils, PI Merlin Méheut). This work was performed using HPC resources from CALMIP (Calcul en Midi-Pyrénées; grant 2020-P1037).

AlKhatib M. and Eisenhauer A. (2017) Calcium and strontium isotope fractionation in aqueous solutions as a function of temperature and reaction rate; I. Calcite. *Geochimica et Cosmochimica Acta* **209**, 296–319.

Althoff P. (1977) Structural refinements of dolomite and a magnesian calcite and implications for dolomite formation in the marine environment. *American Mineralogist* **62**, 772–783.

Antonelli M.A., Schiller M., Schauble E.A., Mittal T., DePaolo D.J., Chacko T., Grew E.S. and Tripoli B. (2019) Kinetic and equilibrium Ca isotope effects in high-T rocks and minerals. *Earth and Planetary Science Letters* **517**, 71–82.

Baer M.D. and Mundy C.J. (2016) Local Aqueous Solvation Structure Around Ca2+ During Ca2+···Cl– Pair Formation. *The Journal of Physical Chemistry B* **120**, 1885–1893. PMID: 26788746.

Baldereschi A. (1973) Mean-Value Point in the Brillouin Zone **7**, 5212.

Barone V., Casarin M., Forrer D., Pavone M., Sambi M. and Vittadini A. (2009) Role and effective treatment of dispersive forces in materials: Polyethylene and graphite crystals as test cases. *Journal of Computational Chemistry* **30**, 934–939.

Baroni S., de Gironcoli S. and Corso A.D. (2001) Phonons and related crystal properties from density-functional theory **73**, 515–562.

Becke A.D. (1988) Density-functional exchange-energy approximation with correct asymptotic behavior. *Phys. Rev. A* **38**, 3098–3100.

Becke A.D. (1993) Density-functional thermochemistry. III. The role of exact exchange. *The Journal of Chemical Physics* **98**, 5648–5652.

Cameron M., Sueno S., Prewitt C.T. and Papike J.J. (1973) High-temperature crystal chemistry of acmite, diopside, hedenbergite, jadeite,spodumene, and ureyite. *American Mineralogist* **58**, 594–618.

Caspi E.N., Pokroy B., Lee P.L., Quintana J.P. and Zolotoyabko E. (2005) On the structure of aragonite. *Acta Crystallographica Section B* **61**, 129–132.

Chizhik V.I., Egorov A.V., Pavlova M.S., Egorova M.I. and Donets A.V. (2016) Structure of hydration shell of calcium cation by NMR relaxation, Car-Parrinello molecular dynamics and quantum-chemical calculations. *Journal of Molecular Liquids* **224**, 730 – 736.

Colla C.A., Wimpenny J., Yin Q.Z., Rustad J.R. and Casey W.H. (2013) Calcium-isotope fractionation between solution and solids with six, seven or eight oxygens bound to Ca(II). *Geochimica et Cosmochimica Acta* **121**, 363 – 373.

Dal Corso A. (2014) Pseudopotentials periodic table: From H to Pu. *Computational Materials Science* **95**, 337 – 350.

De La Pierre M., Demichelis R. and Dovesi R. (2016) *Vibrational Spectroscopy of Minerals Through Ab Initio Methods*, John Wiley & Sons, Ltd, chapter 10. pp. 341–374.

Demichelis R., Raiteri P. and Gale J.D. (2017) *Ab Initio Modelling of the Structure and Properties of Crystalline Calcium Carbonate*, Springer International Publishing, Cham. pp. 113–135.

DePaolo D.J. (2011) Surface kinetic model for isotopic and trace element fractionation during precipitation of calcite from aqueous solutions **75**, 1039 – 1056.

Ducher M., Pietrucci F., Balan E., Ferlat G., Paulatto L. and Blanchard M. (2017) van der Waals Contribution to the Relative Stability of Aqueous Zn(2+) Coordination States. *Journal of Chemical Theory and Computation* **13**, 3340–3347. PMID: 28621954.

Dupuis R., Benoit M., Nardin E. and Méheut M. (2015) Fractionation of silicon isotopes in liquids: The importance of configurational disorder. *Chemical Geology* **396**, 239 – 254.

Effenberger H., Mereiter K. and Zemann J. (1981) Crystal structure refinements of magnesite, calcite, rhodochrosite, siderite, smithonite, and dolomite, with discussion of some aspects of the stereochemistry of calcite type carbonates. *Zeitschrift für Kristallographie - Crystalline Materials*

719 **156**, 233 – 244.

720 Fantle M.S. and DePaolo D.J. (2007) Ca isotopes in carbonate sediment and pore fluid from ODP
721 Site 807A: The Ca2+(aq)–calcite equilibrium fractionation factor and calcite recrystallization
722 rates in Pleistocene sediments. *Geochimica et Cosmochimica Acta* **71**, 2524–2546.

723 Feng C., Qin T., Huang S., Wu Z. and Huang F. (2014) First-principles investigations of equilibrium
724 calcium isotope fractionation between clinopyroxene and Ca-doped orthopyroxene. *Geochimica*
725 *et Cosmochimica Acta* **143**, 132–142. The Subduction Factory: Geochemical Perspectives.

726 Füger A., Méheut M., Mavromatis V., Leis A. and Dietzel M. (2018) Oxygen isotope fractionation
727 during smithsonite formation from aqueous solutions. *Chemical Geology* **495**, 76 – 89.

728 Geiger C.A. and Armbruster T. (1997) $Mn_3Al_2Si_3O_{12}$ spessartine and $Ca_3Al_2Si_3O_{12}$ grossular
729 garnet: structural dynamic and thermodynamic properties. *Am. Mineral.* **82**, 740–747.

730 Giannozzi P., Baroni S., Bonini N., Calandra M., Car R., Cavazzoni C., Ceresoli D., Chiarotti
731 G.L., Cococcioni M., Dabo I., Corso A.D., de Gironcoli S., Fabris S., Fratesi G., Gebauer R.,
732 Gerstmann U., Gougoussis C., Kokalj A., Lazzeri M., Martin-Samos L., Marzari N., Mauri F.,
733 Mazzarello R., Paolini S., Pasquarello A., Paulatto L., Sbraccia C., Scandolo S., Sclauzero G.,
734 Seitsonen A.P., Smogunov A., Umari P. and Wentzcovitch R.M. (2009) QUANTUM ESPRESSO:
735 a modular and open-source software project for quantum simulations of materials **21**, 395502.

736 Grimme S. (2004) Accurate description of van der Waals complexes by density functional theory
737 including empirical corrections. *Journal of Computational Chemistry* **25**, 1463–1473.

738 Grimme S. (2006) Semiempirical GGA-type density functional constructed with a long-range dis-
739 persion correction. *Journal of Computational Chemistry* **27**, 1787–1799.

740 Gussone N., Eisenhauer A., Heuser A., Dietzel M., Bock B., Böhm F., Spero H.J., Lea D.W., Bijma
741 J. and Nägler T.F. (2003) Model for kinetic effects on calcium isotope fractionation (δ^{44}Ca) in
742 inorganic aragonite and cultured planktonic foraminifera. *Geochimica et Cosmochimica Acta*
743 **67**, 1375–1382.

744 Gussone N., Schmitt A.D., Heuser A., Wombacher F., Dietzel M., Tipper E., Schiller M. and Bohm
745 F. (2016) *Calcium stable isotope geochemistry*. Springer.

746 Hamann D.R. (1997) H_2O hydrogen bonding in density-functional theory **55**, 10157.

747 Hohenberg P. and Kohn W. (1964) Inhomogeneous electron gas **136**, 864–871.

748 Holmden C. (2009) Ca isotope study of Ordovician dolomite, limestone, and anhydrite in the
749 Williston Basin: Implications for subsurface dolomitization and local Ca cycling. *Chemical*

Geology **268**, 180–188.

Hossain F., Dlugogorski B., Kennedy E., Belova I. and Murch G. (2011) First-principles study of the electronic, optical and bonding properties in dolomite. *Computational Materials Science* **50**, 1037–1042.

Huang F., Zhou C., Wang W., Kang J. and Wu Z. (2019) First-principles calculations of equilibrium Ca isotope fractionation: Implications for oldhamite formation and evolution of lunar magma ocean. *Earth and Planetary Science Letters* **510**, 153 – 160.

Jacobson A.D. and Holmden C. (2008) d44Ca evolution in a carbonate aquifer and its bearing on the equilibrium isotope fractionation factor for calcite. *Earth and Planetary Science Letters* **270**, 349–353.

Karki B.B. and Wentzcovitch R.M. (2003) Vibrational and quasiharmonic thermal properties of CaO under pressure. *Phys. Rev. B* **68**, 224304.

Kleinman L. and Bylander D.M. (1982) Efficacious form for model pseudopotentials **48**, 1425–1428.

Kohn W. and Sham L. (1965) Self-Consistent Equations Including Exchange and Correlation Effects **140**, A1133–A1138.

Kristyán S. and Pulay P. (1994) Can (semi) local density functional theory account for the London dispersion forces? **229**, 175–180.

Lee C., Vanderbilt D., Laasonen K., Car R. and Parinello M. (1992) Ab initio studies on high-pressure phases of ice **69**, 462–465.

Lee C., Yang W. and Parr R.G. (1988) Development of the Colle-Salvetti correlation-energy formula into a functional of the electron density. *Phys. Rev. B* **37**, 785–789.

Lee K., Murray E.D., Kong L., Lundqvist B.I. and Langreth D.C. (2010) Higher-accuracy van der Waals density functional. *Phys. Rev. B* **82**, 081101.

Medeiros S., Albuquerque E., Maia F., Caetano E. and Freire V. (2006) Structural, electronic, and optical properties of CaCO3 aragonite. *Chemical Physics Letters* **430**, 293–296.

Medeiros S.K., Albuquerque E.L., Maia F.F., Caetano E.W.S. and Freire V.N. (2007) Electronic and optical properties of CaCO3calcite, and excitons in Si@CaCO3and CaCO3@SiO2core-shell quantum dots. *Journal of Physics D: Applied Physics* **40**, 5747–5752.

Méheut M., Lazzeri M., Balan E. and Mauri F. (2007) Equilibrium isotopic fractionation in the kaolinite, quartz, water system: predictions from first-principles density-functional theory **71**, 3170–3181.

781 Méheut M., Lazzeri M., Balan E. and Mauri F. (2009) Structural control over equilibrium silicon
782 and oxygen isotopic fractionation: A first-principles density-functional theory study **258**, 28 –
783 37. Applications of non-traditional stable isotopes in high-temperature geochemistry.
784 Méheut M., Lazzeri M., Balan E. and Mauri F. (2010) First-principles calculation of H/D isotopic
785 fractionation between hydrous minerals and water **74**, 3874 – 3882.
786 Méheut M. and Schauble E.A. (2014) Silicon isotope fractionation in silicate minerals: Insights
787 from first-principles models of phyllosilicates, albite and pyrope. *Geochimica et Cosmochimica*
788 *Acta* **134**, 137 – 154.
789 Mehl M.J., Cohen R.E. and Krakauer H. (1988) Linearized augmented plane wave electronic struc-
790 ture calculations for MgO and CaO. *Journal of Geophysical Research: Solid Earth* **93**, 8009–8022.
791 Monkhorst H.J. and Pack J.D. (1976) Special points for Brillouin-zone integrations **13**, 5188–5192.
792 Moynier F. and Fujii T. (2017) Calcium isotope fractionation between aqueous compounds relevant
793 to low-temperature geochemistry, biology and medicine. *Scientific Reports* **7**, 44255.
794 Méheut M., Ibañez-Mejia M. and Tissot F.L. (2021) Drivers of zirconium isotope fractionation in
795 Zr-bearing phases and melts: The roles of vibrational, nuclear field shift and diffusive effects.
796 *Geochimica et Cosmochimica Acta* **292**, 217–234.
797 Oelkers E.H., Pogge von Strandmann P.A. and Mavromatis V. (2019) The rapid resetting of the
798 Ca isotopic signatures of calcite at ambient temperature during its congruent dissolution, pre-
799 cipitation, and at equilibrium. *Chemical Geology* **512**, 1–10.
800 Perdew J.P. (1986) Density-functional approximation for the correlation energy of the inhomoge-
801 neous electron gas. *Phys. Rev. B* **33**, 8822–8824.
802 Perdew J.P., Burke K. and Ernzerhof M. (1996) Generalized gradient approximation made simple
803 **77**, 3865–3868.
804 Perdew J.P., Ruzsinszky A., Csonka G.I., Vydrov O.A., Scuseria G.E., Constantin L.A., Zhou
805 X. and Burke K. (2008) Restoring the Density-Gradient Expansion for Exchange in Solids and
806 Surfaces. *Phys. Rev. Lett.* **100**, 136406.
807 Perdew J.P. and Zunger A. (1981) Self-interaction correction to density-functional approximations
808 for many-electron systems. *Phys. Rev. B* **23**, 5048–5079.
809 Perez-Fernandez A., Berninger U.N., Mavromatis V., Pogge von Strandmann P. and Oelkers E.
810 (2017) Ca and Mg isotope fractionation during the stoichiometric dissolution of dolomite at
811 temperatures from 51 to 126°C and 5bars CO2 pressure. *Chemical Geology* **467**, 76–88.

Richet P., Bottinga Y. and Javoy M. (1977) A review of hydrogen, carbon, nitrogen, oxygen, and chlorine stable isotope fractionation among gaseous molecules. *Annu. Rev. Earth Planet. Sci.* **5**, 65–110.

Rustad J.R., Casey W.H., Yin Q.Z., Bylaska E.J., Felmy A.R., Bogatko S.A., Jackson V.E. and Dixon D.A. (2010) Isotopic fractionation of $Mg^{2+}_{(aq)}$, $Ca^{2+}_{(aq)}$, and $Fe^{2+}_{(aq)}$ with carbonate minerals **74**, 6301 – 6323.

Schauble E.A., Ghosh P. and Eiler J.M. (2006) Preferential formation of $^{13}C-^{18}O$ bonds in carbonate minerals, estimated using first-principles lattice dynamics **70**, 2510–2529.

Schmitt A.D. (2016) *Calcium stable isotope geochemistry*, Springer Berlin Heidelberg, Berlin, Heidelberg, chapter Earth-Surface Ca Isotopic Fractionations. pp. 145–172.

Speziale S., Shieh S.R. and Duffy T.S. (2006) High-pressure elasticity of calcium oxide: A comparison between Brillouin spectroscopy and radial X-ray diffraction. *Journal of Geophysical Research: Solid Earth* **111**.

Stamm F.M., Méheut M., Zambardi T., Chmeleff J., Schott J. and Oelkers E.H. (2020) Extreme silicon isotope fractionation due to Si organic complexation: Implications for silica biomineralization. *Earth and Planetary Science Letters* **541**, 116287.

Troullier N. and Martins J. (1991) Efficient pseudopotentials for plane-wave calculations. **43**, 1993–2006.

Tsuchiya T., Tsuchiya J., Umemoto K. and Wentzcovitch R.M. (2004) Phase transition in MgSiO3 perovskite in the earth's lower mantle. *Earth and Planetary Science Letters* **224**, 241 – 248.

Valenzano L., Noël Y., Orlando R., Zicovich-Wilson C.M., Ferrero M. and Dovesi R. (2007) Ab initio vibrational spectra and dielectric properties of carbonates: magnesite, calcite and dolomite. *Theoretical Chemistry Accounts* **117**, 991–1000.

Wang W., Qin T., Zhou C., Huang S., Wu Z. and Huang F. (2017a) Concentration effect on equilibrium fractionation of Mg-Ca isotopes in carbonate minerals: Insights from first-principles calculations. *Geochimica et Cosmochimica Acta* **208**, 185–197.

Wang W., Zhou C., Qin T., Kang J.T., Huang S., Wu Z. and Huang F. (2017b) Effect of Ca content on equilibrium Ca isotope fractionation between orthopyroxene and clinopyroxene. *Geochimica et Cosmochimica Acta* **219**, 44–56.

Tables

Table 1: β-factors (in ‰) calculated at 300K with the PBEsol functional and various samplings of the Brillouin zone.

mineral	$\ln\beta$ exact	$\ln\beta_{\Gamma}$	$\ln\beta_{2\times2\times2}$
CaO	15.60	5.88	15.68
calcite	13.33	12.21	
dolomite	12.43	11.17	
aragonite	10.41	9.63	
diopside	13.45	12.55	
grossular	17.61	17.44	

Table 2: Fractionation properties (raw and corrected) calculated at 300K for the different materials and within the various theoretical schemes tested in this study, showing their variability. For each material, the first line gives the raw calculated β-factor, the second gives the β-factor corrected for the frequency error using the average relative error $\overline{\chi}$ (Eq.(11)), the third gives the β-factor corrected for the frequency error using Eq.(10) . The functional spread represents the width of the interval obtained with the results of the different theoretical schemes for a given mineral, either raw or corrected.

	PZ	PBE	vdW-DF2	BLYP	BLYP+D2	PBEsol	spread
				$\ln \beta_{mineral}$(‰)			
CaO	16.97	14.38	14.56	13.86	14.96	15.60	3.11
	17.02	16.64	16.48	16.43	16.70	16.92	0.59
	16.63	16.25	16.31	16.08	16.40	16.54	0.55
calcite	15.35	12.05	13.27	11.76	12.78	13.33	3.59
	15.12	12.52	13.29	12.09	13.31	13.65	3.02
	13.49	13.78	13.60	13.57	13.84	13.90	0.41
dolomite	14.14	11.25	12.27	10.93	12.05	12.43	3.21
	13.68	12.11	12.97	11.95	12.59	12.86	1.74
	12.83	12.20	12.35	11.80	12.35	12.70	1.03
aragonite	12.21	9.10	10.13	8.59	9.23	10.41	3.62
	11.70	10.59	11.40	10.16	10.58	11.11	1.54
	10.86	10.68	10.94	10.56	10.79	10.93	0.39
grossular	19.36	16.28	17.06	15.93	16.36	17.61	3.43
	19.63	18.36	18.89	18.18	17.98	18.99	1.65
	19.39	18.56	18.93	18.40	18.22	18.99	1.17
diopside	14.86	12.53	13.17	12.45	13.53	13.45	2.41
	14.95	13.99	14.28	14.08	14.49	14.41	0.96
	14.58	14.00	14.10	14.15	14.33	14.27	0.58
				$\ln \alpha_{mineral-calcite}$(‰)			
CaO	1.63	2.33	1.29	2.10	2.18	2.27	1.04
	1.91	4.12	3.19	4.34	3.39	3.27	2.43
	3.15	2.47	2.70	2.52	2.55	2.64	0.67

dolomite	-1.21	-0.80	-1.00	-0.83	-0.72	-0.90	0.48
	-1.43	-0.41	-0.32	-0.15	-0.71	-0.80	1.29
	-0.66	-1.59	-1.26	-1.77	-1.49	-1.20	1.11
aragonite	-3.13	-2.95	-3.14	-3.17	-3.55	-2.92	0.63
	-3.42	-1.93	-1.89	-1.93	-2.73	-2.54	1.52
	-2.63	-3.12	-2.66	-3.00	-3.05	-2.97	0.48
grossular	4.02	4.23	3.79	4.17	3.58	4.28	0.70
	4.52	5.84	5.59	6.09	4.68	5.33	1.57
	5.90	4.77	5.33	4.84	4.38	5.08	1.52
diopside	-0.49	0.48	-0.10	0.69	0.75	0.12	1.24
	-0.17	1.47	0.99	1.99	1.19	0.75	2.16
	1.09	0.21	0.49	0.59	0.49	0.37	0.89

Table 3: Functional spread obtained for each mineral pair before/after correction. Colors emphasize minerals for which correction is assumed less precise due to inhomogeneous experimental sampling of their vibrational properties. green: mineral fully characterized (CaO, dolomite). Orange: calcite, ≈25% "orphan" contribution. Red: grossular, ≈55% "orphan" contribution. Black: aragonite and diopside, ≈10% "orphan" contribution.

	CaO	dolomite	aragonite	diopside	calcite	grossular
CaO		0.9/0.5	1.3/0.4	0.8/0.3	1.0/0.7	1.1/0.9
dolomite			0.9/0.7	0.8/0.8	0.5/1.1	0.9/0.7
aragonite				1.7/0.6	0.6/0.5	0.4/1.1
diopside					1.2/0.9	1.7/0.9
calcite						0.7/1.5
grossular						

Table 4: Recommended fits of $1000\ln\beta^{44/40}Ca_{mineral}$ and of $1000\ln\alpha^{44/40}Ca_{mineral-calcite}$ for 0-1200°C, based on ax^2+bx^3 with $x=\frac{10^2}{T(K)}$. We used the raw PBEsol results (see text for discussion).

System	Fit parameters	
	a	b
$1000\ln\beta^{44/40}Ca_{mineral}$		
calcite	127.9	-23.9
dolomite	119.5	-23.1
aragonite	99.1	-16.4
CaO	148.2	-23.6
grossular	171.2	-38.1
diopside	129.8	-26.3
$1000\ln\alpha^{44/40}Ca_{mineral-calcite}$		
dolomite	-8.4	0.8
aragonite	-28.8	7.5
CaO	20.3	0.3
grossular	43.3	-14.2
diopside	1.9	-2.4

Table 5: Comparison of the isotope fractionation properties calculated here with literature. R10: Rustad et al. (2010); FH: Fang Huang et al. (Wang et al., 2017a; Wang et al., 2017b; Huang et al., 2019); A19: Antonelli et al. (2019)

property	this work	R10	FH	A19
preferred isotope fractionation values at 300K				
$\ln \alpha^{44/40}\mathrm{Ca}_{dolomite-calcite}$	-0.9	-2.3	-1.1	
$\ln \alpha^{44/40}\mathrm{Ca}_{aragonite-calcite}$	-2.9		-2.8	
$\ln \alpha^{44/40}\mathrm{Ca}_{grossular-diopside}$	4.2		5.8	4.4
$\ln \alpha^{44/40}\mathrm{Ca}_{grossular-lime}$	2.0			2.2
isotope fractionations at 300K calculated with BP86				
$\ln \beta_{calcite}$	12.26	16.01		
isotope fractionations at 300K calculated with PZ				
$\ln \alpha^{44/40}\mathrm{Ca}_{dolomite-calcite}$	-1.2		-1.1	
$\ln \alpha^{44/40}\mathrm{Ca}_{aragonite-calcite}$	-3.1		-2.8	
$\ln \alpha^{44/40}\mathrm{Ca}_{grossular-diopside}$	4.5		5.8	
$\ln \beta^{44/40}\mathrm{Ca}_{calcite}$	15.34		15.81	
$\ln \beta^{44/40}\mathrm{Ca}_{dolomite}$	14.14		14.74	
$\ln \beta^{44/40}\mathrm{Ca}_{aragonite}$	12.21		13.01	
$\ln \beta^{44/40}\mathrm{Ca}_{diopside}$	14.86		15.51	
$\ln \beta^{44/40}\mathrm{Ca}_{grossular}$	19.36		21.31	

Table 6: Lattice parameters (in Å and °) and average Ca-O bond lengths (in Å) calculated with the PZ functional, here and in the literature, and comparison with experiment. The numbers in parenthesis refer to uncertainties on the last significant digit. For each distance, Δ is the relative difference (in %) between the experimental and calculated value. FH: Fang Huang & al. (Feng et al., 2014: diopside; Wang et al., 2017a: calcite, dolomite, aragonite; Huang et al., 2019: grossular); Others: Karki and Wentzcovitch (2003) for CaO, Medeiros et al. (2007) for calcite, Hossain et al. (2011) for dolomite, Medeiros et al. (2006) for aragonite ; AE: all electron (Mehl et al., 1988 for CaO)

	this work:		FH		Others		AE		$\text{Exp}^{(a-f)}$
	value	Δ	value	Δ	value	Δ	value	Δ	
lime CaO									
a	4.7157	-2.0			4.703	-2.3	4.714	-2.0	4.8115[5]
Ca-O	2.358	-2.0			2.351	-2.3	2.357	-2.0	2.4058[3]
calcite									
a	4.9614	-0.6	5.0037	+0.2	4.957	-0.7			4.9896[2]
c	16.4176	-3.8	16.6114	-2.6	16.416	-3.8			17.0610[11]
Ca-O	2.3121	-2.0	2.341	-0.8	2.311	-2.0			2.3598[6]
dolomite									
a	4.7714	-0.7	4.8005	-0.1	4.787	-0.3			4.8033[9]
c	15.5651	-2.6	15.5833	-2.5	15.55	-2.7			15.984[4]
Ca-O	2.3315	-2.0	2.361	-0.7	2.328	-2.1			2.378[1]
aragonite									
a	4.8863	-1.5	4.9210	-0.8	4.893	-1.4			4.96183[1]

Table 6: (continued)

:								
b	7.8346	-1.7	7.9282	-0.5	7.850	-1.5		7.96914[2]
c	5.5381	-3.6	5.5822	-2.8	5.523	-3.8		5.74285[2]
Ca-O	2.4692	-2.3	2.491	-1.4				2.5272 [5]
				grossular				
a	11.7000	-1.2	11.776	-0.6				11.847[1]
Ca-O	2.3711	-1.4	2.393	-0.5				2.405[1]
				diopside				
a	9.6478	-1.0	9.689	-0.6				9.746[4]
b	8.7739	-1.4	8.828	-0.8				8.899[5]
c	5.1996	-1.0	5.211	-0.8				5.251[6]
$\beta(^\circ)$	105.77		105.263					105.63[6]
Ca-O	2.4547	-1.7	2.470	-1.1				2.4976

(a) CaO: Speziale et al. (2006)

(b) calcite: Effenberger et al. (1981) X-ray diffraction

at ambient temperature

(c) dolomite: Althoff (1977) X-ray diffraction

(d) aragonite: Caspi et al. (2005) Synchrotron Hi-Res X-Ray

(e) grossular: Geiger and Armbruster (1997) X-ray diffraction at 293K

(f) diopside: Cameron et al. (1973) X-ray diffraction

at ambient temperature

Table 7: Comparison of the $\ln \beta^{44/40}$Ca calculated at 300K (PBEsol functional) with structural parameters of the different structures (estimated on experimental structures). Ca-O: average Ca-O distances. Vol: volume of the coordination polyhedra. D: Baur's distortion index on distances. Qel: quadratic elongation of the coordination polyhedra. BAV: bond angle variance. Coord: coordination.

mineral	Ca-O	Vol	D	Qel	BAV	coord	$\ln \beta$
	Å	Å^3			°^{2}		‰
calcite	2.3574	17.414	0	1.0020	7.4660	6	13.33
dolomite	2.3815	17.960	0	1.0017	6.1194	6	12.43
CaO lime	2.4075	18.605		1.0000	0	6	15.60
aragonite	2.5283	29.808	0.0258			9	10.41
grossular	2.4019	23.765	0.0335			8	17.61
diopside	2.4976	25.757	0.0567			8	13.45

List of Figures

Figures

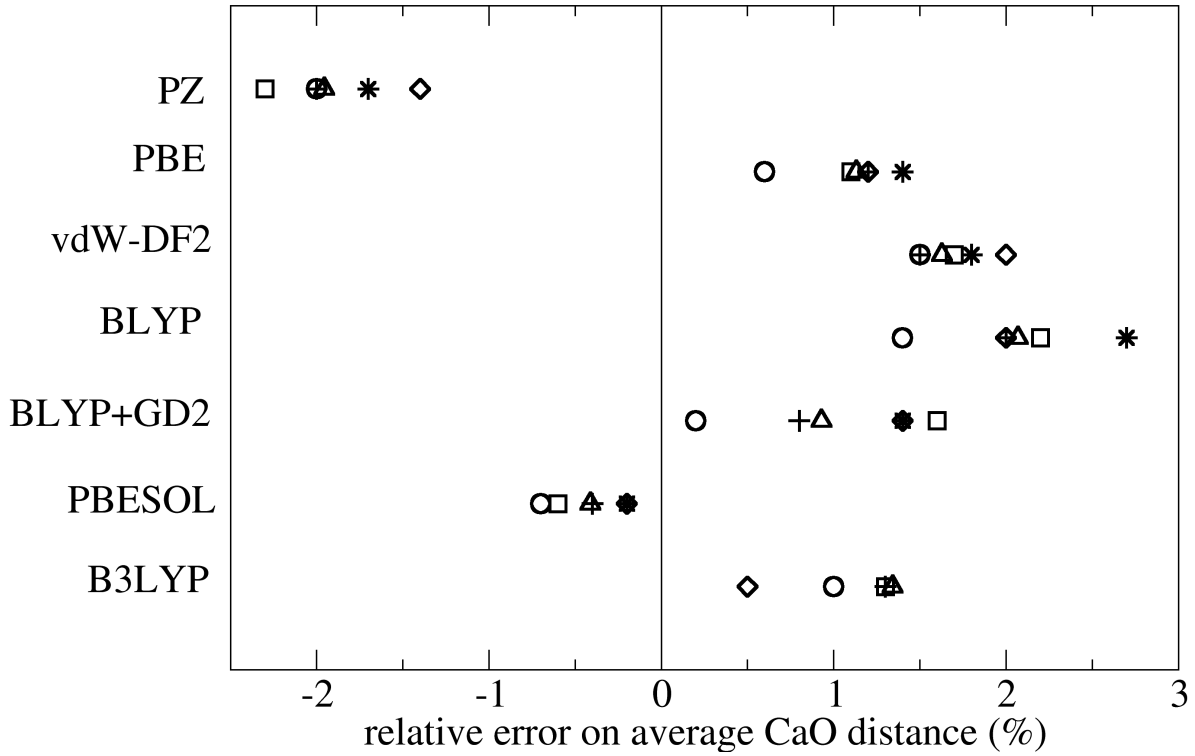

Fig. 1: Relative difference $\frac{<Ca-O>_{th}}{<Ca-O>_{exp}} - 1$ (in %) between average CaO distances of relaxed structures ($< Ca - O >_{th}$) and measurements ($< Ca - O >_{exp}$), for CaO lime ($\circ$), calcite ($+$), dolomite ($\triangle$) aragonite ($\square$), grossular ($\diamond$), and diopside ($\star$). See Table EA-1 for raw data. Note the better (closer to 0%) and more consistent (less dispersion between minerals) results obtained with the PBEsol calculation.

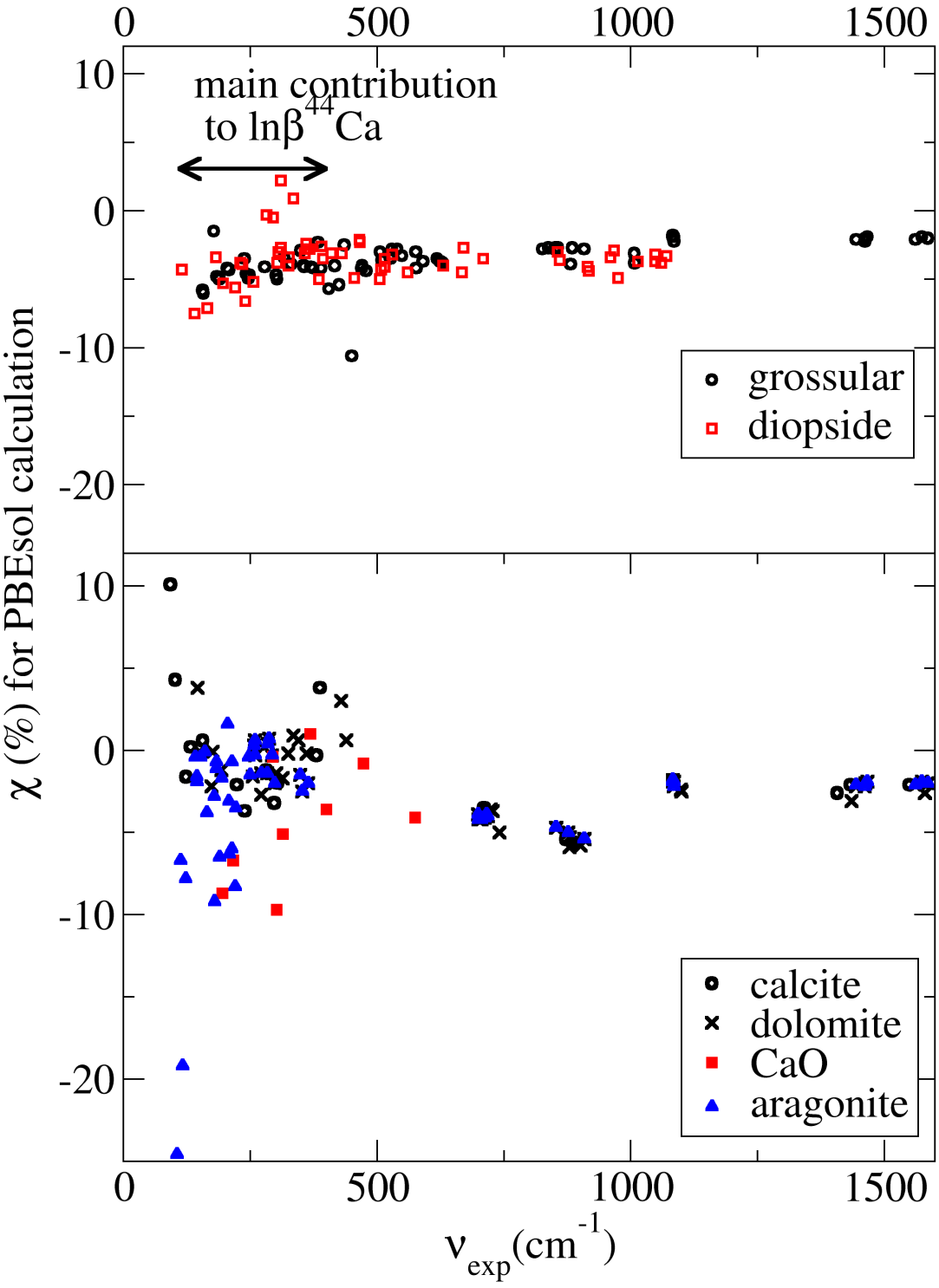

Fig. 2: Theoretical frequency offset χ (in %) as a function of experimental frequency, for calculations with the PBEsol functional. As seen on Fig.5, the range of frequencies most important for Ca isotope fractionation properties are between 100 and 400 cm^{-1} (double arrow) .

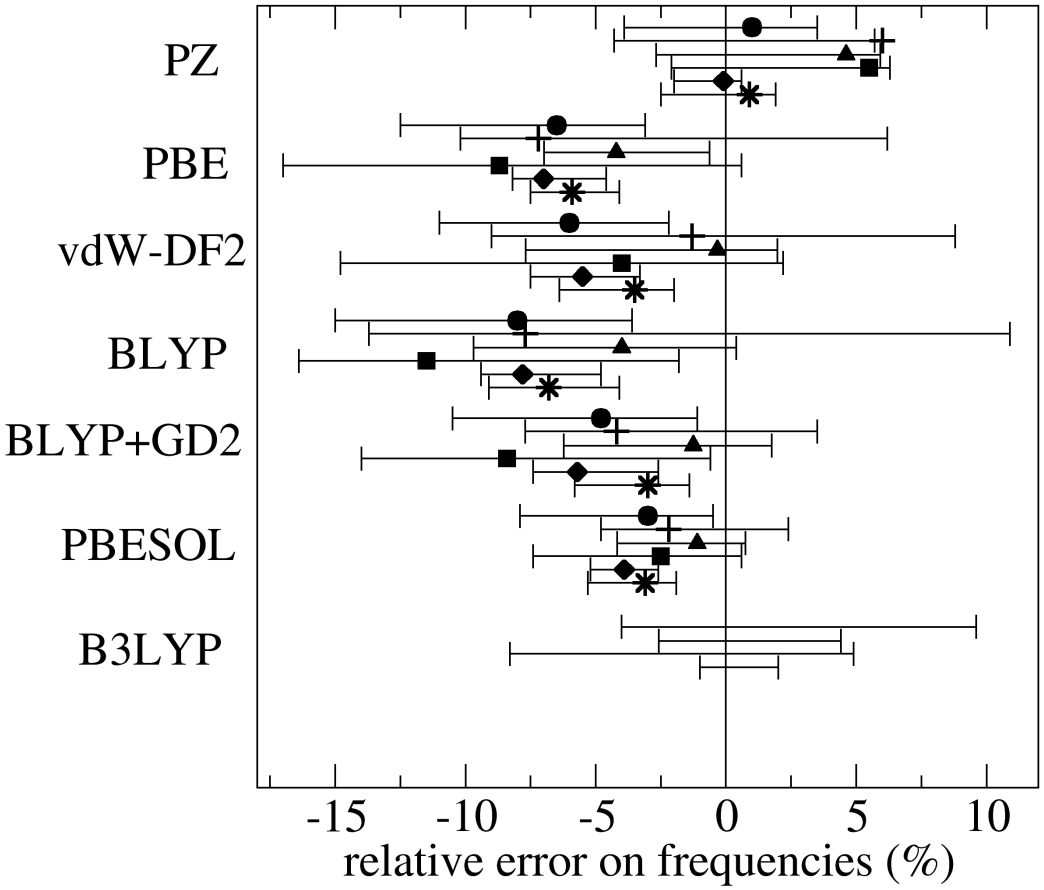

Fig. 3: Frequency offset $\chi = \frac{\nu_{calc}}{\nu_{exp}} - 1$ (in %) between calculation and experimental frequencies. Error bars represent the $\overline{\chi} \pm \sigma(\chi)$ uncertainty interval for χ, whereas symbols indicate $\overline{\chi}^h$, for CaO lime (●), calcite (+), dolomite(▲),aragonite (■), grossular (◆), and diopside (⋆). The four B3LYP uncertainty intervals correspond to calcite, dolomite, aragonite and grossular, from top to bottom. See Tables EA-2 to EA-7 for raw data. Note the smaller uncertainty on χ for diopside and grossular. Note also the good efficiency of the PBEsol calculation, giving smaller uncertainty on χ (smaller $\sigma(\chi)$ for a given material), and smaller variability on $\overline{\chi}^h$.

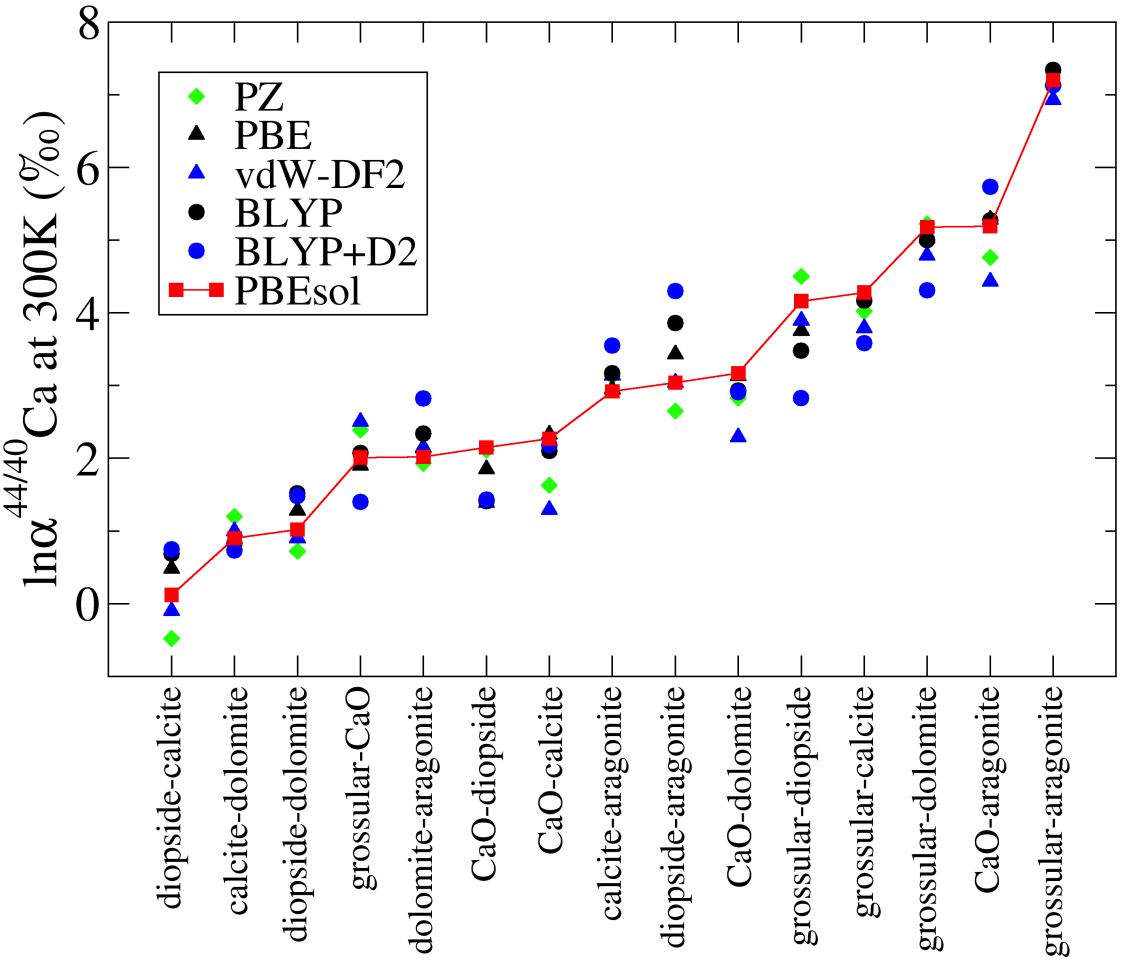

Fig. 4: Fractionation calculated at 300K for all the 15 mineral pairs considered in this work. The pair order is chosen (between A-B and B-A) to give a positive fractionation in PBEsol. The pairs are ordered by increasing value of the fractionation calculated in PBEsol.

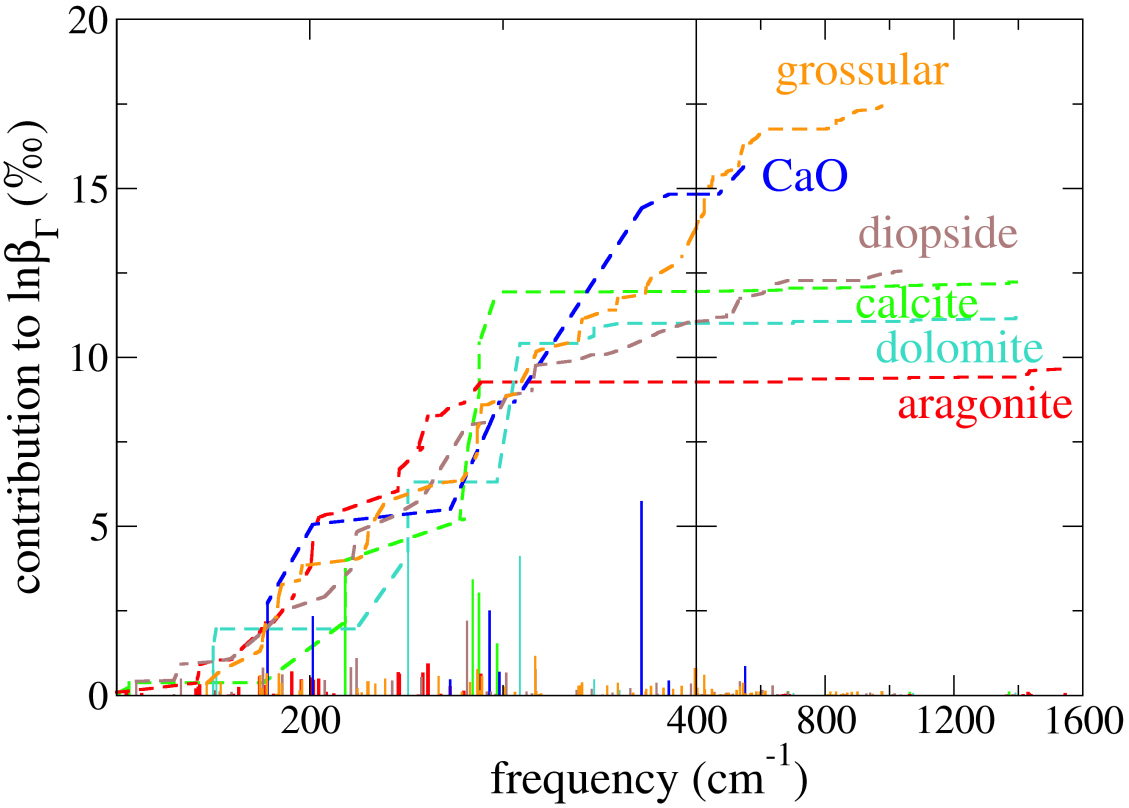

Fig. 5: Plot of the contribution h (bars, in ‰) of individual frequencies to $\ln\beta_\Gamma$ at 300K, for the PBEsol calculations. Dashed lines are integrated contributions, converging towards $\ln\beta_\Gamma$.

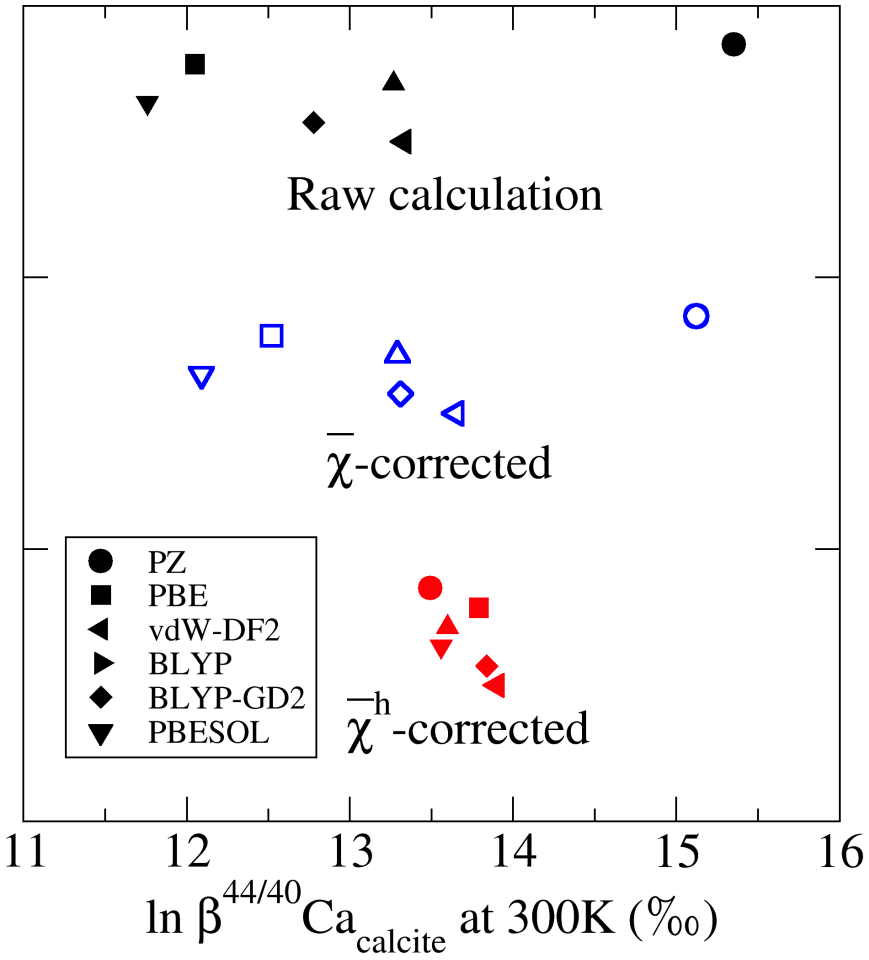

Fig. 6: Logarithmic β-factors calculated at 25°C for calcite and within the various approximate functionals tested in this study. Black filled symbols : raw calculated properties; Blue empty symbols: properties corrected for the frequency error using the average relative error $\overline{\chi}$ (Eq.(11)). Red: properties corrected for the frequency error using Eq.(10)

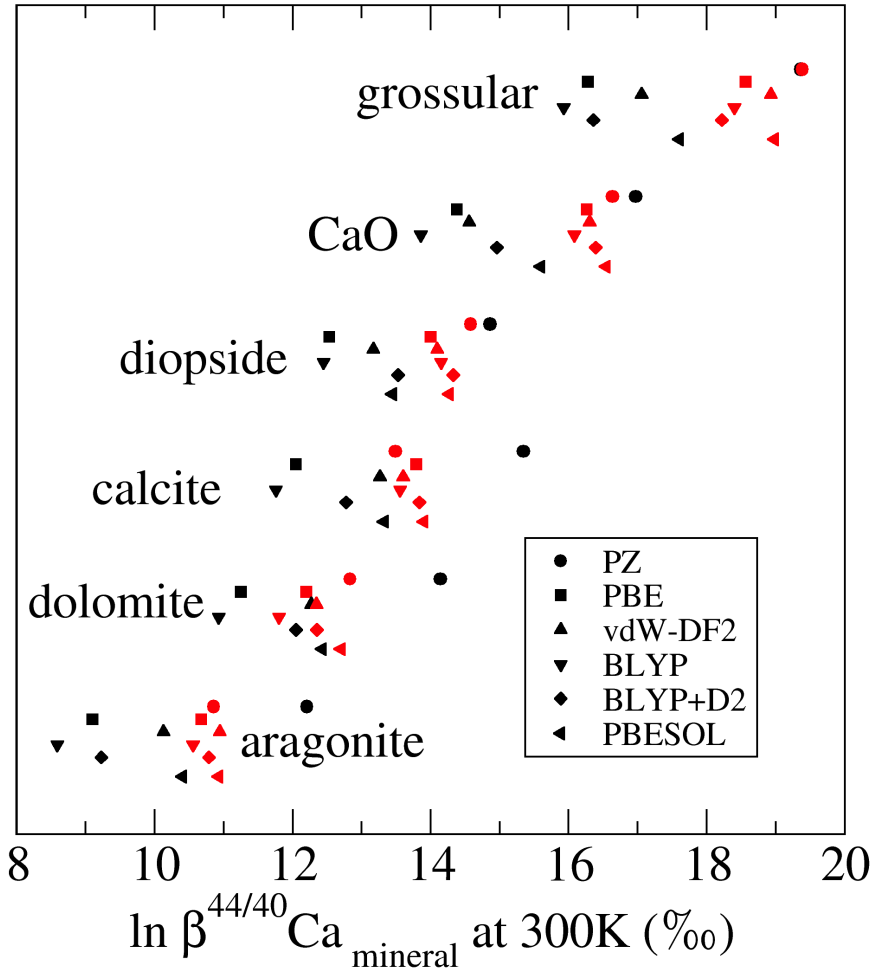

Fig. 7: Logarithmic β-factors calculated for the different materials and within the various approximate functionals tested in this study. Black filled symbols : raw calculated properties; Red: properties corrected for the frequency error using Eq.(10)

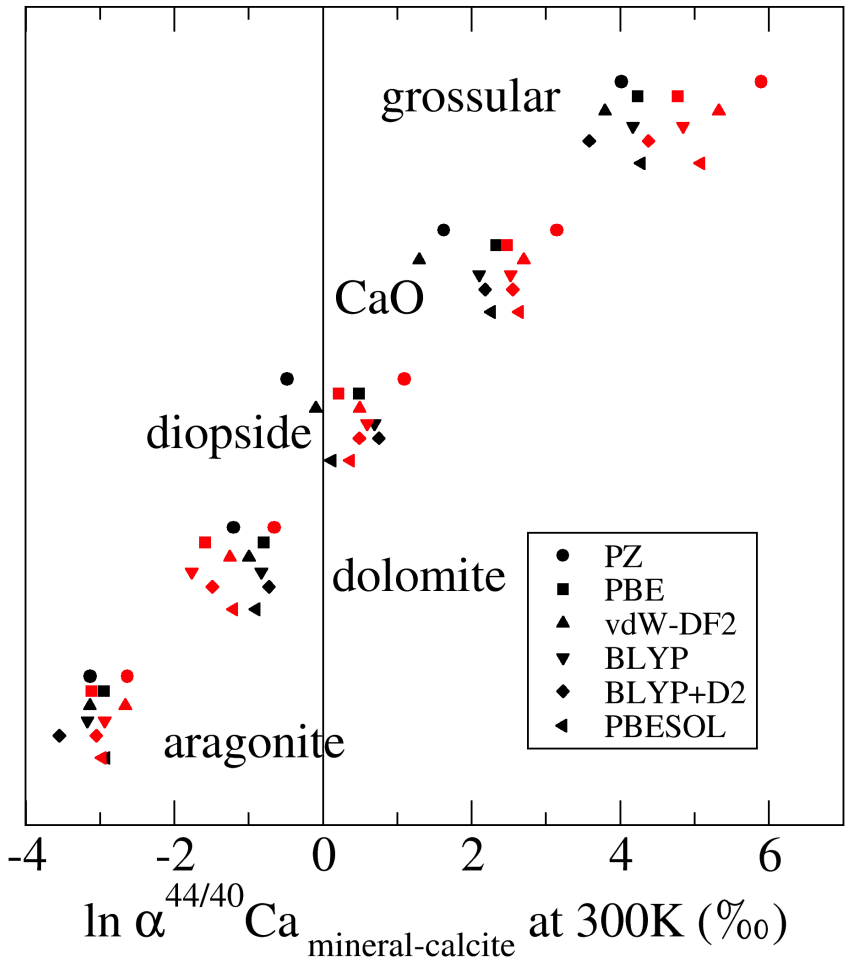

Fig. 8: Calculated fractionation factors relative to calcite for the different materials and within the various approximate functionals tested in this study. Black: "raw" calculated properties; Red: properties corrected for the frequency error using Eq.8 (see text)

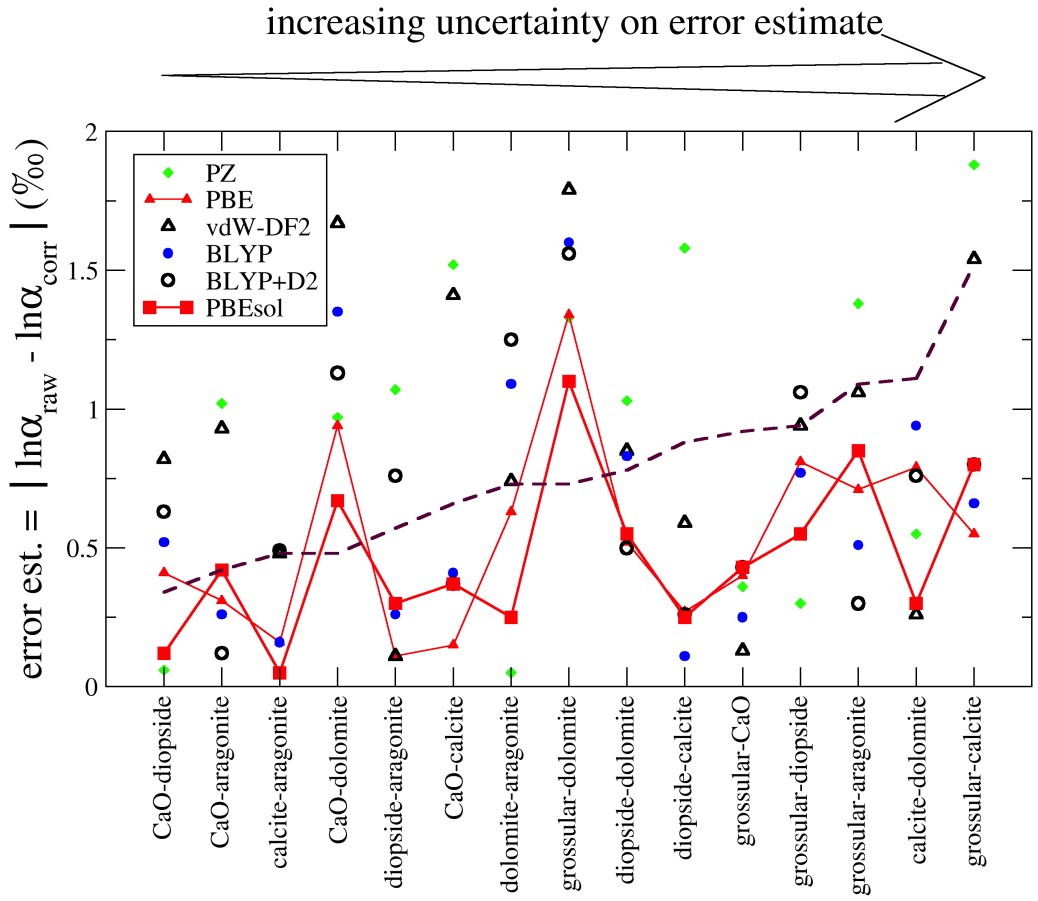

Fig. 9: Errors on calculated isotope fractionation properties ($\ln \alpha^{44/40}$Ca), as estimated by the absolute difference between the "raw" calculation for a given mineral pair and a given theoretical scheme, and the corrected calculation for the same pair and scheme. Symbols indicate PBEsol (■), BLYP-D2 (○), BLYP (●), vdW-DF2 (△), PBE (▲), and PZ (◆). The estimated errors appear by increasing order of uncertainty, as measured by the functional spread after correction (dashed line, see Table 3 and discussion in 4.2.2). See Table 2, for raw data.

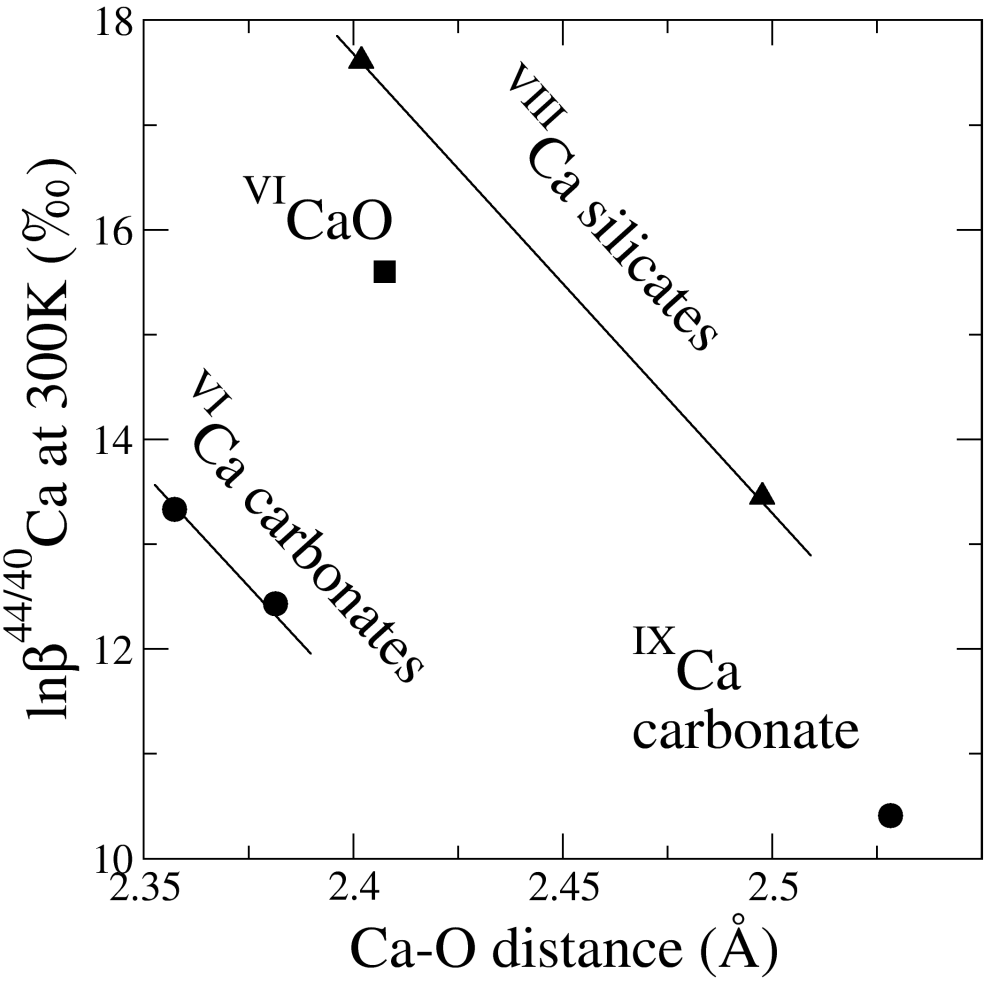

Fig. 10: Calculated isotope fractionation properties (logarithmic β-factors at 300K) as a function of mean CaO distance for the various minerals considered here. Coordination is given in Roman number.

ELECTRONIC ANNEX

Table EA-1: Experimental (exp, from literature) and calculated lattice parameters and Ca-O distances (this work, and from literature for B3LYP calculation) in Å and °, for the materials considered here. The numbers in parenthesis refer to uncertainties on the last significant digit. For each distance, Δ(%) is the relative difference between the experimental and calculated value.

	Exp$^{(a-f)}$	PZ:		PBE		vdW-DF2		BLYP		BLYP+GD2		PBESOL		B3LYP$^{(g-k)}$	
		value	Δ(%)	value	Δ(%)	value	Δ(%)	value	Δ(%)	value	Δ(%)	value	Δ(%)		
lime CaO															
a	4.8115[5]	4.7157		4.8382		4.8822		4.8781		4.8180		4.7746		4.858	
Ca-O	2.4058[3]	2.358	-2.0	2.419	+0.6	2.441	+1.5	2.439	+1.4	2.409	+0.2	2.387	-0.7	2.429	+1.0
calcite															
a	4.9896[2]	4.9614	-0.6	5.0602	+1.4	5.0930	+2.1	5.0929	+2.1	5.0643	+1.5	5.0099	+0.4	5.0373	+1.0
c	17.0610[11]	16.4176	-3.8	17.2059	+0.8	17.1122	+0.3	17.3614	+1.8	17.0348	-0.2	16.8516	-1.2	17.3304	+1.6
Ca-O	2.3598[6]	2.3121	-2.0	2.3871	+1.2	2.3941	+1.5	2.4072	+2.0	2.3792	0.8	2.3504	-0.4	2.3907	+1.3
dolomite															
a	4.8033[9]	4.7714	-0.7	4.8662	+1.3	4.8894	+1.8	4.8943	+1.9	4.8626	+1.2	4.8216	+0.4	4.8376	+0.7
c	15.984[4]	15.5651	-2.6	16.2415	+1.6	16.2287	+1.5	16.4176	+2.7	16.0957	+0.7	15.9324	-0.3	16.2756	+1.8
Ca-O	2.378[1]	2.3315	-2.0	2.4049	+1.1	2.4167	+1.6	2.4272	+2.1	2.4001	+0.9	2.3682	-0.4	2.4099	+1.3
aragonite															
a	4.96183[1]	4.8863	-1.5	5.0173	+1.1	5.0543	+1.9	5.0581	+1.9	5.0677	+2.1	4.9517	-0.2	5.008	+0.9
b	7.96914[2]	7.8346	-1.7	8.0433	+0.9	8.0513	+1.0	8.1074	+1.7	8.0516	+1.0	7.9406	-0.4	8.029	+0.8
c	5.74285[2]	5.5381	-3.6	5.8239	+1.4	5.8540	+1.9	5.9162	+3.0	5.8192	+1.3	5.6768	-1.2	5.861	+2.1
Ca-O	2.5272 [5]	2.4692	-2.3	2.5562	+1.1	2.5689	+1.7	2.5838	+2.2	2.5679	+1.6	2.5120	-0.6	2.560	+1.3
grossular															
a	11.847[1]	11.7000	-1.2	11.9923	+1.2	12.0535	+1.7	12.0651	+1.8	11.9986	+1.3	11.8471	=	11.9368	+0.8
Ca-O	2.405[1]	2.3711	-1.4	2.4332	+1.2	2.4530	+2.0	2.4538	+2.0	2.4383	+1.4	2.4007	-0.2	2.4180	+0.5
diopside															
a	9.746[4]	9.6478	-1.0	9.9031	+1.6	9.9232	+1.8	10.0017	+2.6	9.8583	+1.2	9.7752	+0.3	9.8931	+1.5
b	8.899[5]	8.7739	-1.4	9.0448	+1.6	9.0594	+1.8	9.1242	+2.5	9.0183	+1.3	8.9151	+0.2	9.0199	+1.4
c	5.251[6]	5.1996	-1.0	5.3375	+1.6	5.3430	+1.8	5.3926	+2.7	5.3254	+1.4	5.2661	+0.3	5.3265	+1.4
β	105.63[6]	105.77		106.46		105.86		107.01		105.68		106.05		106.37	
Ca-O	2.4976	2.4547	-1.7	2.5335	+1.4	2.5418	+1.8	2.5662	+2.7	2.5325	+1.4	2.4930	-0.2	2.5350	+1.5
Δ_{CaO} interval (%)		-1.85±0.45		+1±0.4		+1.75±0.25		+2.05±0.65		+0.9±0.7		-0.45±0.25		+1±0.5	

(a) CaO: Speziale et al. (2006)
(b) calcite: Effenberger et al. (1981) X-ray diffraction
at ambient temperature
(c) dolomite: Althoff (1977) X-ray diffraction
(d) aragonite: Caspi et al. (2005) Synchrotron Hi-Res X-Ray
(e) grossular: Geiger and Armbruster (1997) X-ray diffraction at 293K
(f) diopside: Cameron et al. (1973) X-ray diffraction
at ambient temperature
(g) CaO: Calculated from cell volumes at 0K extracted from Figure 4 of Erba et al. (2015)
(h) calcite: Valenzano et al. (2007), BSD basis set
(i) dolomite: Valenzano et al. (2007), BSD basis set
(h) aragonite: Carteret et al. (2013)
(j) grossular: Zicovich-Wilson et al. (2008)
(k) diopside: Prencipe (2012)

Table EA-2: Modelled vibrational frequencies ν (in cm^{-1}) of lime CaO at Γ, X and L, and comparison to experiment. Measurements (Exp) are compiled from Saunderson and Peckham (1971), Vijayaraghavan et al. (1972), and Rieder et al. (1973) Values of lnβ and h (in ‰) are computed at 300K for the $^{44/40}$Ca pair. χ is the deviation (in %) between the theoretical frequency and its experimental counterpart.

	PZ			PBE			vdW-DF2			BLYP			BLYP+GD2			PBESOL			exp
	ν	χ (%)	h (‰)	ν	χ (%)	h (‰)	ν	χ (%)	h (‰)	ν	χ (%)	h (‰)	ν	χ (%)	h (‰)	ν	χ (%)	h (‰)	
Γ_{TO}	291.1	-3.6	0.51	254.5	-15.7	0.39	261.6	-13.4	0.42	245.2	-18.8	0.37	260.2	-13.8	0.41	272.6	-9.7	0.45	302
Γ_{LO}	569.4	-1.0	0.90	536.2	-6.7	0.81	537.9	-6.4	0.81	531.5	-7.6	0.80	547.5	-4.8	0.84	551.3	-4.1	0.85	575
X_{TA}	205.3	-4.9	2.33	197.5	-8.6	2.33	197.4	-8.6	2.33	195.7	-9.4	2.36	199.0	-7.9	2.31	201.5	-6.7	2.33	216
X_{LA}	311.1	5.8	2.90	276.6	-5.9	2.17	284.3	-3.3	2.36	269.7	-8.3	2.04	288.1	-2.0	2.43	292.9	-0.4	2.49	294
X_{TO}	315.6	0.5	0.98	283.0	-9.9	0.39	293.0	-6.7	0.44	277.5	-11.6	0.23	292.5	-6.8	0.56	298.0	-5.1	0.68	314
X_{LO}	393.2	-1.7	0.27	381.9	-4.5	0.52	387.6	-3.1	0.42	383.8	-4.1	0.58	386.2	-3.5	0.38	385.7	-3.6	0.42	400
L_{TA}	189.0	-3.1	3.07	167.2	-14.2	2.41	168.9	-13.4	2.46	161.4	-17.2	2.25	172.1	-11.8	2.55	178.0	-8.7	2.73	195
L_{LA}	382.5	3.9	6.06	361.5	-1.8	5.43	359.9	-2.2	5.39	356.9	-3.0	5.31	365.3	-0.7	5.54	371.6	1.0	5.73	368
L_{TO}	323.9		0.00	289.6		0.00	295.2		0.00	283.5		0.00	298.0		0.00	305.7		0.00	
L_{LO}	485.7	2.7	0.00	457.6	-3.3	0.00	461.7	-2.3	0.00	456.0	-3.6	0.00	468.8	-0.9	0.00	469.2	-0.8	0.00	473
$\sum h = \ln\beta_{2\times2\times2}$			17.02			14.45			14.63			13.94			15.02			15.68	
$\ln\beta_{exact}$			16.97			14.38			14.56			13.86			14.96			15.60	
$\overline{\chi}$		-0.2			-7.8			-6.6			-9.3			-5.8			-4.2		
$\sigma(\chi)$		3.7			4.7			4.4			5.7			4.7			3.7		
$\overline{\chi}^{h\,\dagger}$		1.0			-6.5			-6.0			-8.0			-4.8			-3.0		

$\dagger\overline{\chi}^{h} = \frac{\sum \chi\times h}{\sum h}$

Table EA-3: Modelled vibrational modes (frequencies ν in cm^{-1} and intensities) for calcite, and comparison to experiment. PBE refers to the present calculations. Measurements (Exp) are compiled from Gillet et al. (1993), Deines (2004) for Raman, and Gillet et al. (1996) for Infrared. Values of lnβ and h (in ‰) are computed at 300K for the $^{44/40}$Ca pair. χ is the deviation (in %) between the theoretical frequency and its experimental counterpart. .

sym.	PZ:			PBE			vdW-DF2			BLYP			BLYP+GD2			PBESOL			BP			Exp	B3LYP[(a)]	
	ν	χ (%)	h (‰)	ν	χ (%)	h (‰)	ν	χ (%)	h (‰)	ν	χ (%)	h (‰)	ν	χ (%)	h (‰)	ν	χ (%)	h (‰)	ν	χ (%)	h (‰)	ν	ν	χ (%)
Raman																								
E_g	166.9	7.0	0.00	151.5	-2.9	0.00	160.7	3.0	0.00	151.7	-2.8	0.00	155.9	-0.1	0.00	156.9	0.6	0.00	152.8	-2.1	0.00	156	152.9	-2.0
E_g	297.8	6.0	0.00	263.8	-6.1	0.00	277.6	-1.2	0.00	259.8	-7.5	0.00	270.8	-3.6	0.00	277.6	-1.2	0.00	265.2	-5.6	0.00	281	276.8	-1.5
E_g	695.9	-2.0	0.00	679.7	-4.3	0.00	680.8	-4.1	0.00	676.3	-4.7	0.00	679.7	-4.3	0.00	685.0	-3.5	0.00	678.4	-4.4	0.00	710	705.0	-0.7
E_g	1427.9	-0.4	0.00	1372.0	-4.3	0.00	1314.4	-8.3	0.00	1329.3	-7.2	0.00	1344.5	-6.2	0.00	1402.7	-2.1	0.00	1363.1	-4.9	0.00	1433	1438.5	0.4
A_{1g}	1082.6	=	0.00	1045.0	-3.5	0.00	1017.4	-6.1	0.00	1023.3	-5.5	0.00	1032.0	-4.7	0.00	1063.2	-1.8	0.00	1040.2	-3.9	0.00	1083	1081.7	-0.1
Infrared																								
E_u TO	**98.6**	**-3.3**	**0.24**	**116.5**	**14.2**	**0.35**	**121.0**	**18.6**	**0.37**	**127.0**	**24.5**	**0.41**	**112.8**	**10.6**	**0.31**	**106.4**	**4.3**	**0.28**	**118.0**	**15.7**	**0.35**	**102**	**117.7**	**15.4**
E_u LO	114.9	-6.5		129.2	5.0		133.4	8.5		137.7	11.9		126.1	2.5		121.0	-1.6		130.4	6.0		123	135	9.8
E_u TO	**238.1**	**6.8**	**4.28**	**205.2**	**-8.0**	**3.21**	**219.5**	**-1.6**	**3.66**	**202.8**	**-9.1**	**3.13**	**213.6**	**-4.2**	**3.49**	**218.3**	**-2.1**	**3.62**	**207.5**	**-6.9**	**3.29**	**223**	**225.2**	**1.0**
E_u LO	250.8	4.9		216.2	-9.5		231.3	-3.2		213.0	-10.9		224.9	-5.9		230.2	-3.7		218.4	-8.6		239	236	-1.3
E_u TO	**314.6**	**5.9**	**3.66**	**267.8**	**-9.8**	**2.60**	**286.9**	**-3.4**	**3.03**	**261.6**	**-11.9**	**2.49**	**280.2**	**-5.7**	**2.91**	**287.5**	**-3.2**	**3.02**	**270.6**	**-8.9**	**2.67**	**297**	**293.7**	**-1.1**
E_u LO	399.8	5.2		364.1	-4.2		373.5	-1.7		358.7	-5.6		373.8	-1.6		378.9	-0.3		365.8	-3.7		380	378	-0.5
E_u TO	695.1	-2.1	0.17	679.8	-4.4	0.07	681.3	-4.2	0.09	676.5	-4.9	0.05	679.9	-4.4	0.08	684.7	-3.7	0.10	678.5	-4.6	0.07	711	706.3	-0.7
E_u LO	697.3	-2.1		681.0	-4.2		682.2	-4.1		677.4	-4.7		681.0	-4.2		686.4	-3.5		679.7	-4.4		711	708	-0.4
E_u TO	1392.7	-1.0	0.08	1341.3	-4.7	0.10	1280.9	-9.0	0.10	1298.4	-7.7	0.11	1312.3	-6.7	0.11	1370.5	-2.6	0.09	1331.8	-5.3	0.10	1407	1406.9	-0.0
E_u LO	1543.0	-0.4		1486.2	-4.1		1433.1	-7.5		1445.5	-6.7		1461.4	-5.7		1516.7	-2.1		1477.8	-4.6		1549	1551	0.1
A_{2u} TO	89.0	-3.3	0.07	113.5	23.4	0.12	115.4	25.4	0.12	124.2	35	0.14	104.6	13.7	0.10	101.3	10.1	0.09	113.7	23.6	0.12	92	113.8	23.7
A_{2u} LO	123.9	-6.1		141.7	7.4		145.6	10.3		149.9	13.6		135.5	2.6		132.2	0.2		141.5	7.2		132	149	12.9
A_{2u} TO	**324.9**	**7.2**	**1.84**	**275.7**	**-9.0**	**1.27**	**295.5**	**-2.5**	**1.46**	**268.2**	**-11.5**	**1.19**	**287.8**	**-5.0**	**1.41**	**296.9**	**-2.0**	**1.52**	**278.3**	**-8.2**	**1.31**	**303**	**308.4**	**1.8**
A_{2u} LO	423.2	9.4		385.1	-0.5		393.4	1.7		377.6	-2.4		392.9	1.5		401.6	3.8		386.3	-0.2		387	399	3.1
A_{2u} TO	829.8	-4.8	0.00	823.4	-5.6	0.00	815.9	-6.4	0.00	821.6	-5.8	0.00	820.1	-6.0	0.00	824.5	-5.4	0.00	821.3	-5.8	0.00	872	862.9	-1.0
A_{2u} LO	848.4	-4.7		837.6	-5.9		832.8	-6.4		836.4	-6.0		836.2	-6.0		840.1	-5.6		835.9	-6.1		890	882	-0.9
Silent																								
A_{1u}	**296.6**		**3.70**	**274.4**		**3.18**	**278.4**		**3.27**	**270.4**		**3.10**	**275.1**		**3.20**	**284.2**		**3.41**	**275.3**		**3.21**		**288.9**	
A_{1u}	1081.5		0.10	1044.4		0.07	1017.2		0.08	1022.8		0.07	1031.3		0.08	1062.4		0.08	1039.7		0.07		1082.8	
A_{2g}	175.7		0.00	180.0		0.00	187.3		0.00	184.8		0.00	179.1		0.00	175.8		0.00	180.6		0.00		180.3	
A_{2g}	332.0		0.00	299.3		0.00	308.8		0.00	294.3		0.00	306.3		0.00	312.2		0.00	299.4		0.00		306.3	
A_{2g}	836.6		0.00	828.3		0.00	823.4		0.00	827.8		0.00	826.6		0.00	829.4		0.00	826.3		0.00		869.2	
$\sum h = \ln\beta_{\Gamma}$			14.14			10.97			12.18			10.69			11.69			12.21			11.19			
$\sum_{orphan} h$			3.8			3.25			3.35			3.17			3.61			3.49			3.28			
$\ln\beta_{exact}$			15.34			12.05			13.27			11.76			12.78			13.33			12.26			
$\overline{\chi}$		0.7			-2.0			-0.1			-1.4			-2.1			-1.2					2.8		
$\sigma(\chi)$		5.0			8.2			8.9			12.3			5.6			3.6					6.8		
$\overline{\chi}^{h\,\dagger}$		6.0			-7.2			-1.3			-7.7			-4.2			-2.2							

$\dagger\overline{\chi}^{h} = \frac{\sum \chi\times h}{\sum h}$

(a) De La Pierre et al. (2016)

Table EA-4: (continued)

sym.	PZ: ν	χ (%)	h (‰)	PBE ν	χ (%)	h (‰)	vdW-DF2 ν	χ (%)	h (‰)	BLYP ν	χ (%)	h (‰)	BLYP+GD2 ν	χ (%)	h (‰)	PBESOL ν	χ (%)	h (‰)	Exp ν	B3LYP[(a)] ν	χ (%)

Table EA-4: Modelled vibrational modes (frequencies ν in cm^{-1}) for dolomite and comparison to experiment. Measurements (Exp) are compiled from Matas et al. (2000), Hellwege et al. (1970) and Böttcher et al. (1997) (see Table 6 of Valenzano et al., 2007). Values of lnβ and h (in ‰) are computed at 300K for the $^{44/40}$Ca pair. χ is the deviation (in %) between the theoretical frequency and its experimental counterpart. .

sym.	PZ: ν	χ (%)	h (‰)	PBE ν	χ (%)	h (‰)	vdW-DF2 ν	χ (%)	h (‰)	BLYP ν	χ (%)	h (‰)	BLYP+GD2 ν	χ (%)	h (‰)	PBESOL ν	χ (%)	h (‰)	Exp ν	B3LYP[(a)] ν	χ (%)
Raman																					
E_g	187.1	6.3	0.00	169.1	-3.9	0.00	175.9	-0.0	0.00	167.5	-4.8	0.00	179.1	1.8	0.00	175.9	-0.1	0.00	176	177.0	
E_g	316.3	5.1	0.00	283.3	-5.9	0.00	292.4	-2.9	0.00	277.7	-7.7	0.00	292.6	-2.8	0.00	296.8	-1.4	0.00	301	295.5	
E_g	710.1	-1.9	0.00	692.4	-4.4	0.00	693.0	-4.3	0.00	688.3	-4.9	0.00	694.7	-4.0	0.00	698.2	-3.6	0.00	724	722.5	
E_g	1437.0	-0.5	0.00	1380.5	-4.4	0.00	1322.2	-8.4	0.00	1338.1	-7.3	0.00	1356.0	-6.1	0.00	1411.6	-2.2	0.00	1444	1437.7	
A_g	229.4		0.00	224.6		0.00	232.9		0.00	227.3		0.00	232.6		0.00	224.0		0.00		235.2	
A_g	357.8	6.8	0.00	325.3	-2.9	0.00	332.3	-0.8	0.00	319.8	-4.5	0.00	336.6	0.5	0.00	337.9	0.9	0.00	335	335.8	
A_g	840.8	-4.5	0.00	833.0	-5.3	0.00	827.4	-6.0	0.00	831.6	-5.5	0.00	832.6	-5.4	0.00	833.2	-5.3	0.00	880	888.2	
A_g	1091.5	-0.7	0.00	1054.6	-4.0	0.04	1026.3	-6.6	0.00	1033.6	-6.0	0.00	1044.4	-5.0	0.00	1072.2	-2.4	0.00	1099	1101.0	
Infrared																					
E_u TO	**150.7**	**0.5**	**1.33**	**153.3**	**2.2**	**1.69**	**160.5**	**7.0**	**1.76**	**159.0**	**6.0**	**1.96**	**159.7**	**6.5**	**1.69**	**149.9**	**-0.1**	**1.43**	**150**	**165.3**	
E_u LO	170.1	-1.7		172.5	-0.3		178.4	3.1		177.6	2.7		177.8	2.8		169.2	-2.2		173	186.9	
E_u TO	**269.4**	**5.6**	**5.33**	**238.6**	**-6.4**	**3.48**	**250.2**	**-1.9**	**3.96**	**235.5**	**-7.6**	**3.08**	**247.8**	**-2.8**	**4.09**	**250.8**	**-1.6**	**4.34**	**255**	**256.1**	
E_u LO	284.4	4.9		248.7	-8.2		259.5	-4.2		243.2	-10.3		259.7	-4.2		263.7	-2.7		271	264.5	
E_u TO	**376.7**	**9.2**	**0.57**	**322.7**	**-6.5**	**0.37**	**330.6**	**-4.2**	**0.50**	**311.6**	**-9.7**	**0.33**	**341.0**	**-1.2**	**0.42**	**347.0**	**0.6**	**0.45**	**345**	**339.4**	
E_u LO	464.2	5.7		424.8	-3.2		429.3	-2.2		417.1	-5.0		440.0	0.2		441.7	0.6		439	449.6	
E_u TO	713.7	-2.0	0.09	695.4	-4.5	0.03	696.5	-4.3	0.04	691.4	-5.0	0.02	698.4	-4.1	0.03	701.4	-3.7	0.05	728	726.6	
E_u LO	717.1	-3.2		697.6	-5.9		698.3	-5.8		693.1	-6.5		700.4	-5.5		704.1	-5.0		741	729.1	
E_u TO	1413.5	-1.5	0.06	1360.5	-5.2	0.07	1300.4	-9.4	0.07	1318.2	-8.1	0.08	1335.2	-7.0	0.08	1390.2	-3.1	0.07	1435	1416.5	
E_u LO	1566.0	-0.9		1508.7	-4.5		1456.1	-7.8		1469.0	-7.0		1487.2	-5.9		1539.2	-2.6		1580	1581.5	
A_u TO	**151.3**	**3.6**	**0.51**	**155.7**	**6.6**	**0.62**	**162.5**	**11.3**	**0.67**	**162.8**	**11.5**	**0.72**	**157.3**	**7.8**	**0.63**	**151.5**	**3.8**	**0.54**	**146**	**158.6**	
A_u LO	192.0	-0.5		193.7	0.3		200.4	3.8		198.8	3.0		196.5	1.8		190.7	-1.2		193	204.7	
A_u TO	**328.2**	**4.5**	**4.84**	**292.6**	**-6.8**	**3.31**	**304.1**	**-3.1**	**3.71**	**285.0**	**-9.2**	**2.87**	**300.3**	**-4.4**	**3.67**	**308.7**	**-1.7**	**4.10**	**314**	**302.7**	
A_u LO	339.0	4.3		313.4	-3.6		318.0	-2.2		308.6	-5.1		316.1	-2.7		324.5	-0.2		325	321.4	
A_u TO	**383.0**	**6.1**	**0.00**	**342.1**	**-5.2**	**0.42**	**343.6**	**-4.8**	**0.24**	**332.6**	**-7.9**	**0.62**	**351.5**	**-2.6**	**0.17**	**360.1**	**-0.2**	**0.14**	**361**	**353.8**	
A_u LO	462.8	7.9		425.4	-0.8		427.3	-0.4		415.5	-3.2		435.5	1.5		442.1	3.0		429	439.5	
A_u TO	832.3	-5.3	0.00	826.7	-6.0	0.00	818.2	-6.9	0.00	823.9	-6.3	0.00	824.9	-6.2	0.00	826.7	-5.9	0.00	879	877.6	
A_u LO	858.1	-4.8		846.5	-6.1		841.3	-6.6		844.4	-6.3		847.1	-6.0		848.5	-5.8		901	904.8	
A_u TO	1091.7	-0.8	0.06	1054.7	-4.1	0.00	1026.7	-6.7	0.05	1033.4	-6.1	0.04	1044.3	-5.1	0.05	1072.5	-2.5	0.05	1100	1096.7	
A_u LO	1091.7			1054.7			1026.7			1033.4			1044.3			1072.5				1096.7	
$\sum h = \ln\beta_\Gamma$			12.79			10.03			11.00			9.72			10.83			11.17			
$\ln\beta_{exact}$			14.14			11.25			12.27			10.93			12.05			12.43			
$\overline{\chi}$		0.9			-4.5			-3.6			-5.4			-2.9			-2.4				0.9
$\sigma(\chi)$		4.6			3.8			5.3			5.5			4.4			3.0				3.5
$\overline{\chi}^{h\,\dagger}$		4.6			-4.2			-0.3			-4.0			-1.3			-1.1				

$\dagger\overline{\chi}^{h} = \frac{\sum \chi \times h}{\sum h}$

(a) Valenzano et al. (2007)

Table EA-5: Modelled Raman-active and IR-active modes (frequencies and intensities) for aragonite, and comparison to experiment. PBE refers to the present calculations. Measurements (Exp) are compiled from Carteret et al. (2013). Note that, contrary to the structure (Pmcn setting), the symmetry assignments are defined based on the Pnma spacegroup, consistently with the more general choice made in the literature. Values of lnβ and h (in‰) are computed at 300K for the $^{44/40}$Ca pair. χ is the deviation (in %) between the theoretical frequency and its experimental counterpart.

sym.	PZ ν	χ (%)	h (‰)	PBE ν	χ (%)	h (‰)	vdW-DF2 ν	χ (%)	h (‰)	BLYP ν	χ (%)	h (‰)	BLYP+GD2 ν	χ (%)	h (‰)	PBESOL ν	χ (%)	h (‰)	Exp ν	B3LYP[(a)] ν	χ (%)
Raman																					
A_g	141.7	0.1	0.17	140.2	-0.9	0.20	142.2	0.5	0.20	138.2	-2.3	0.17	136.6	-3.5	0.20	140.9	-0.4	0.18	141.5	148.7	5.1
A_g	173.0	7.8	0.08	151.3	-5.7	0.00	160.7	0.1	0.01	150.1	-6.5	0.05	152.8	-4.8	0.00	160.4	-0.1	0.03	160.5	161.9	0.9
A_g	**206.9**	**6.8**	**0.73**	**177.3**	**-8.5**	**0.63**	**185.0**	**-4.5**	**0.63**	**171.4**	**-11.6**	**0.48**	**174.6**	**-9.9**	**0.56**	**190.6**	**-1.7**	**0.69**	**193.8**	**195.8**	**1.0**
A_g	**224.1**	**5.0**	**0.65**	**182.0**	**-14.8**	**0.42**	**199.0**	**-6.8**	**0.53**	**173.8**	**-18.6**	**0.48**	**182.0**	**-14.8**	**0.43**	**200.7**	**-6.0**	**0.51**	**213.5**	**205.0**	**-4.0**
A_g	301.6	6.4	0.21	263.2	-7.2	0.06	276.7	-2.4	0.15	254.3	-10.3	0.05	263.8	-6.9	0.10	279.6	-1.4	0.11	283.5	280.2	-1.2
A_g	686.8	-2.6	0.02	670.1	-4.9	0.01	668.1	-5.2	0.01	665.1	-5.6	0.01	665.8	-5.5	0.02	675.8	-4.1	0.02	704.9	704.2	-0.1
A_g	816.2	-4.3	0.00	814.5	-4.5	0.00	804.9	-5.6	0.00	811.9	-4.8	0.00	811.3	-4.9	0.00	812.8	-4.7	0.00	853.0	862.8	1.2

Table EA-5: (continued)

sym.	PZ ν	PZ χ (%)	PZ h (‰)	PBE ν	PBE χ (%)	PBE h (‰)	vdW-DF2 ν	vdW-DF2 χ (%)	vdW-DF2 h (‰)	BLYP ν	BLYP χ (%)	BLYP h (‰)	BLYP+GD2 ν	BLYP+GD2 χ (%)	BLYP+GD2 h (‰)	PBESOL ν	PBESOL χ (%)	PBESOL h (‰)	Exp ν	B3LYP[(a)] ν	B3LYP[(a)] χ (%)
A_g	1084.8	-0.1	0.00	1047.5	-3.5	0.00	1018.6	-6.2	0.00	1027.1	-5.4	0.00	1030.7	-5.0	0.00	1065.3	-1.9	0.00	1085.5	1095.3	0.9
A_g	1455.7	-0.5	0.03	1406.4	-3.9	0.04	1350.	-7.7	0.04	1367.5	-6.5	0.04	1377.4	-5.9	0.04	1433.9	-2.0	0.03	1463.0	1473.9	0.8
B_{1g}	120.6	7.1	0.14	86.8	-22.9	0.06	89.5	-20.5	0.07	66.2	-41.2	0.04	63.7	-43.4	0.03	105.0	-6.7	0.10	112.6	97.4	-13.5
B_{1g}	159.8	5.3	0.00	145.1	-4.4	0.01	155.0	2.2	0.00	143.1	-5.7	0.01	147.0	-3.1	0.00	151.1	-0.4	0.01	151.7	152.1	0.3
B_{1g}	**228.0**		**0.44**	**185.5**		**0.42**	**202.9**		**0.52**	**177.8**		**0.40**	**190.6**		**0.44**	**204.5**		**0.48**		**199.0**	
B_{1g}	231.2	8.1	0.19	199.8	-6.6	0.03	210.4	-1.6	0.00	191.9	-10.3	0.03	206.5	-3.5	0.07	212.5	-0.7	0.04	213.9	213.4	-0.2
B_{1g}	687.0	-2.6	0.04	670.7	-5.0	0.03	671.4	-4.9	0.03	666.6	-5.5	0.03	669.1	-5.2	0.03	676.4	-4.2	0.03	705.7	705.5	=
B_{1g}	1455.0	-0.4	0.08	1397.5	-4.4	0.08	1335.9	-8.6	0.09	1353.8	-7.4	0.09	1358.7	-7.0	0.10	1429.7	-2.2	0.08	1461.5	1463.9	0.2
B_{2g}	**188.6**	**5.5**	**0.64**	**161.5**	**-9.7**	**0.47**	**168.6**	**-5.7**	**0.49**	**154.2**	**-13.8**	**0.41**	**155.9**	**-12.8**	**0.42**	**173.8**	**-2.8**	**0.55**	**178.8**	**182.5**	**2.1**
B_{2g}	221.0	7.8	0.05	198.7	-3.1	0.11	203.1	-1.0	0.10	192.6	-6.1	0.15	195.7	-4.6	0.12	208.4	1.6	0.08	205.1	207.2	1.0
B_{2g}	**259.8**	**5.3**	**0.86**	**235.2**	**-4.7**	**0.54**	**241.3**	**-2.2**	**0.60**	**229.7**	**-6.9**	**0.39**	**234.7**	**-4.9**	**0.55**	**245.7**	**-0.4**	**0.63**	**246.8**	**249.2**	**1.0**
B_{2g}	**277.0**	**6.7**	**0.73**	**243.0**	**-6.4**	**0.42**	**261.3**	**0.7**	**0.81**	**238.9**	**-7.9**	**0.50**	**249.5**	**-3.9**	**0.72**	**258.8**	**-0.3**	**0.66**	**259.5**	**260.7**	**0.5**
B_{2g}	293.1		0.16	263.0		0.43	274.0		0.17	259.5		0.44	269.6		0.12	272.7		0.25		278.7	
B_{2g}	701.6	-2.0	0.01	680.3	-5.0	0.01	677.9	-5.3	0.01	674.1	-5.8	0.01	675.3	-5.7	0.01	688.2	-3.9	0.01	715.8	714.6	-0.2
B_{2g}	870.5	-4.1	0.01	855.4	-5.8	0.00	852.1	-6.2	0.01	852.4	-6.1	0.01	859.8	-5.3	0.01	858.9	-5.4	0.00	908.0	911.8	0.4
B_{2g}	1080.3	-0.4	0.02	1044.1	-3.8	0.01	1015.6	-6.4	0.02	1024.1	-5.6	0.01	1027.8	-5.3	0.01	1061.5	-2.2	0.01	1085.0	1091.6	0.6
B_{2g}	1571.6	-0.2	0.06	1513.5	-3.8	0.05	1461.7	-7.1	0.06	1474.5	-6.3	0.05	1486.2	-5.6	0.06	1544.7	-1.9	0.05	1574.0	1591.8	1.1
B_{3g}	132.4	8.1	0.09	91.1	-25.6	0.02	101.0	-17.6	0.04	72.0	-41.2	0.01	77.0	-37.1	0.01	113.0	-7.8	0.05	122.5	101.3	-17.3
B_{3g}	**176.6**	**-1.7**	**0.07**	**149.7**	**-16.6**	**0.32**	**163.6**	**-8.9**	**0.35**	**140.9**	**-21.5**	**0.31**	**159.6**	**-11.1**	**0.51**	**163.0**	**-9.2**	**0.23**	**179.6**	**167.6**	**-6.7**
B_{3g}	**194.0**	**2.4**	**0.51**	**167.6**	**-11.6**	**0.14**	**177.3**	**-6.4**	**0.16**	**164.6**	**-13.1**	**0.13**	**171.1**	**-9.7**	**0.00**	**177.2**	**-6.5**	**0.29**	**189.5**	**177.8**	**-6.2**
B_{3g}	286.3	5.5	0.06	254.3	-6.3	0.01	269.1	-0.9	0.03	248.2	-8.6	0.01	261.3	-3.8	0.01	267.7	-1.4	0.03	271.5	271.4	=
B_{3g}	679.9	-3.0	0.00	666.9	-4.8	0.00	668.5	-4.6	0.00	663.9	-5.2	0.00	666.0	-4.9	0.00	671.0	-4.2	0.00	700.6	701.2	0.1
B_{3g}	1405.9		0.00	1352.1		0.00	1287.9		0.00	1308.6		0.00	1310.3		0.00	1382.6		0.00		1415.0	
Infrared																					
B_{1u} TO	**148.8**	**3.0**	**0.25**	**137.3**	**-4.9**	**0.24**	**142.7**	**-1.2**	**0.23**	**134.8**	**-6.6**	**0.24**	**138.3**	**-4.2**	**0.23**	**142.1**	**-1.6**	**0.24**	**144.4**	**147.3**	**2.0**
B_{1u} LO	148.9	2.8		137.4	-5.2		142.7	-1.5		135.2	-6.7		138.4	-4.5		142.1	-1.9		144.9	147.4	1.7
B_{1u} TO	**216.0**	**3.5**	**0.58**	**179.7**	**-13.9**	**0.36**	**194.2**	**-6.9**	**0.47**	**173.0**	**-17.1**	**0.31**	**177.2**	**-15.1**	**0.36**	**195.5**	**-6.3**	**0.45**	**208.6**	**200.7**	**-3.8**
B_{1u} LO	234.5	6.0		196.4	-11.3		211.7	-4.4		188.4	-14.9		196.2	-11.3		213.5	-3.5		221.3	218.4	-1.3
B_{1u} TO	**273.0**	**9.4**	**0.82**	**222.9**	**-10.7**	**0.55**	**242.1**	**-3.0**	**0.59**	**212.4**	**-14.9**	**0.52**	**224.5**	**-10.0**	**0.56**	**245.7**	**-1.5**	**0.66**	**249.5**	**245.5**	**-1.6**
B_{1u} LO	376.7	3.4		340.3	-6.6		348.3	-4.4		333.5	-8.4		341.3	-6.3		357.0	-2.0		364.2	359.7	-1.2
B_{1u} TO	311.8	4.6	0.00	280.1	-6.0	0.00	293.0	-1.7	0.00	277.1	-7.0	0.00	292.1	-2.0	0.00	292.1	-2.0	0.00	298.0	293.1	-1.6
B_{1u} LO	311.7	6.5		279.5	-4.5		292.6	-0.1		276.3	-5.6		291.7	-0.4		291.8	-0.3		292.8	292.8	=
B_{1u} TO	695.1	-2.4	0.01	677.1	-5.0	0.01	675.0	-5.2	0.01	671.8	-5.7	0.01	673.0	-5.5	0.01	683.5	-4.1	0.01	712.4	712.2	=
B_{1u} LO	698.2	-2.3		679.0	-5.0		676.3	-5.3		673.2	-5.8		674.2	-5.6		686.0	-4.0		714.4	714.2	=
B_{1u} TO	872.0	-4.0	0.00	856.4	-5.8	0.00	853.3	-6.1	0.00	853.4	-6.1	0.00	860.8	-5.3	0.00	860.1	-5.4	0.00	908.8	913.1	0.5
B_{1u} LO	872.0	-4.0		856.4	-5.8		853.4	-6.1		853.4	-6.1		860.8	-5.3		860.1	-5.4		908.8	913.1	0.5
B_{1u} TO	1082.9	0.0	0.00	1045.5	-3.4	0.00	1017.0	-6.1	0.00	1025.1	-5.3	0.00	1028.7	-5.0	0.00	1063.5	-1.8	0.00	1082.8	1092.9	0.9
B_{1u} LO	1083.0	0.0		1045.7	-3.4		1017.4	-6.0		1025.4	-5.3		1029.0	-5.0		1063.6	-1.8		1082.8	1092.9	0.9
B_{1u} TO	1463.6	-0.2	0.01	1408.5	-4.0	0.02	1351.2	-7.2	0.02	1367.4	-6.8	0.02	1379.0	-6.0	0.02	1439.2	-1.9	0.01	1466.6	1474.1	0.5
B_{1u} LO	1581.7	-0.3		1523.2	-4.0		1472.5	-7.2		1484.2	-6.4		1496.5	-5.6		1554.4	-2.0		1586.0	1602.9	1.1
B_{2u} TO	101.6	-3.6	0.02	46.7	-55.7	0.00	45.7	-56.6	0.00	-43.4			-18.8			79.5	-24.6	0.01	105.4	65.4	-38.0
B_{2u} LO	115.9	-0.5		64.2	-44.9		68.0	-41.6		-16.9			24.9			94.1	-19.2		116.5	83.7	-28.2
B_{2u} TO	173.6	5.7	0.00	146.5	-10.8	0.00	158.0	-3.8	0.00	141.8	-13.6	0.00	147.3	-10.3	0.01	157.9	-3.8	0.00	164.2	158.7	-3.4
B_{2u} LO	173.8	5.8		146.5	-10.8		158.0	-3.8		141.8	-13.6		147.9	-9.9		158.0	-3.8		164.2	158.9	-3.2
B_{2u} TO	**229.1**	**4.2**	**0.57**	**179.0**	**-18.6**	**0.36**	**196.8**	**-10.5**	**0.43**	**167.3**	**-23.9**	**0.33**	**184.7**	**-16.0**	**0.39**	**201.7**	**-8.3**	**0.45**	**219.9**	**198.0**	**-10.0**
B_{2u} LO	362.8	2.9		328.1	-6.9		333.0	-5.5		319.2	-9.4		333.9	-5.3		343.7	-2.5		352.5	343.8	-2.5
B_{2u} TO	680.5	-2.8	0.02	664.4	-5.1	0.01	663.3	-5.2	0.01	659.6	-5.7	0.02	661.2	-5.5	0.02	670.4	-4.2	0.02	699.8	697.4	-0.3
B_{2u} LO	681.8	-2.5		665.1	-4.8		663.6	-5.1		660.0	-5.6		661.4	-5.4		671.5	-3.9		699.0	698.1	-0.1
B_{2u} TO	1440.2	-0.3	0.02	1380.8	-4.4	0.02	1317.9	-8.8	0.02	1335.9	-7.5	0.02	1341.0	-7.2	0.02	1414.1	-2.1	0.02	1444.5	1445.1	=
B_{2u} LO	1555.8	-0.3		1494.4	-4.3		1438.7	-7.8		1452.3	-7.0		1459.0	-6.5		1527.6	-2.1		1561.0	1571.8	0.7
B_{3u} TO	200.2	9.3	0.02	164.4	-10.2	0.04	174.5	-4.7	0.02	154.5	-15.6	0.04	162.4	-11.3	0.03	181.1	-1.1	0.03	183.1	174.1	-4.9
B_{3u} LO	200.6	9.4		166.0	-9.4		175.3	-4.3		156.3	-14.7		163.5	-10.8		182.0	-0.7		183.3	174.6	-4.8
B_{3u} TO	**223.4**	**7.5**	**0.66**	**183.1**	**-11.9**	**0.40**	**199.8**	**-3.8**	**0.52**	**175.5**	**-15.5**	**0.36**	**184.1**	**-11.4**	**0.42**	**201.3**	**-3.1**	**0.51**	**207.8**	**210.1**	**1.1**
B_{3u} LO	358.6	2.9		329.8	-5.3		338.5	-2.9		325.7	-6.5		333.1	-4.4		343.0	-1.5		348.4	353.8	1.6
B_{3u} TO	**273.1**	**5.4**	**0.95**	**252.2**	**-2.7**	**0.96**	**256.4**	**-1.1**	**0.98**	**249.7**	**-3.7**	**1.03**	**251.8**	**-2.9**	**1.04**	**260.8**	**0.6**	**0.92**	**259.2**	**269.1**	**3.8**
B_{3u} LO	269.5	4.8		249.8	-2.9		253.2	-1.6		246.6	-4.1		247.6	-3.7		258.0	0.3		257.2	266.9	3.8
B_{3u} TO	**307.4**	**7.1**	**0.75**	**273.8**	**-4.6**	**0.46**	**281.1**	**-2.0**	**0.47**	**265.1**	**-7.6**	**0.33**	**270.5**	**-5.7**	**0.34**	**288.8**	**0.7**	**0.62**	**286.9**	**288.9**	**0.7**
B_{3u} LO	303.8	6.7		271.6	-4.6		278.8	-2.0		263.5	-7.4		268.8	-5.6		285.8	0.4		284.6	287.0	0.8
B_{3u} TO	701.6	-2.3	0.00	683.6	-4.8	0.00	682.6	-5.0	0.00	679.0	-5.5	0.00	679.8	-5.4	0.00	689.6	-4.0	0.00	718.3	719.2	0.1
B_{3u} LO	701.7	-2.3		683.6	-4.8		682.6	-5.0		679.1	-5.5		679.8	-5.4		689.7	-4.0		718.4	719.2	0.1
B_{3u} TO	815.5	-4.3	0.01	813.7	-4.5	0.00	804.1	-5.6	0.00	811.1	-4.8	0.00	810.5	-4.9	0.00	812.0	-4.7	0.00	852.2	861.9	1.1
B_{3u} LO	840.8	-4.1		831.9	-5.1		824.7	-5.9		829.3	-5.4		830.1	-5.3		833.0	-5.0		876.7	886.7	1.1
B_{3u} TO	1081.4	-0.1	0.02	1044.5	-3.5	0.01	1015.9	-6.2	0.02	1024.4	-5.4	0.01	1027.8	-5.1	0.02	1062.1	-1.9	0.02	1082.8	1092.9	0.9
B_{3u} LO	1082.3	-0.1		1045.2	-3.5		1016.8	-6.1		1025.1	-5.4		1028.6	-5.0		1063.0	-1.9		1083.3	1093.6	1.0
B_{3u} TO	1456.7		0.05	1403.5		0.05	1347.7		0.05	1362.6		0.05	1374.3		0.05	1433.0		0.05		1469.9	
B_{3u} LO	1456.8			1403.5			1347.8			1362.6			1374.3			1433.0				1469.9	
Silent																					
A_u	109.7		0.01	48.0		0.00	46.8		0.00	-49.1			-31.9			83.8		0.01			
A_u	**160.3**		**0.47**	**125.8**		**0.14**	**135.5**		**0.14**	**116.4**		**0.04**	**121.7**		**0.08**	**142.7**		**0.31**			
A_u	**172.1**		**0.08**	**135.0**		**0.22**	**149.4**		**0.29**	**127.4**		**0.28**	**145.0**		**0.33**	**151.3**		**0.13**			
A_u	272.6		0.02	244.9		0.00	258.5		0.00	240.7		0.01	252.2		0.00	256.0		0.00			

Table EA-5: (continued)

sym.	PZ ν	PZ χ (%)	PZ h (‰)	PBE ν	PBE χ (%)	PBE h (‰)	vdW-DF2 ν	vdW-DF2 χ (%)	vdW-DF2 h (‰)	BLYP ν	BLYP χ (%)	BLYP h (‰)	BLYP+GD2 ν	BLYP+GD2 χ (%)	BLYP+GD2 h (‰)	PBESOL ν	PBESOL χ (%)	PBESOL h (‰)	Exp ν	B3LYP[(a)] ν	B3LYP[(a)] χ (%)
A_u	672.5		0.00	659.1		0.00	658.6		0.00	655.0		0.00	655.9		0.00	663.6		0.00			
A_u	1385.0		0.01	1331.3		0.01	1265.9		0.01	1287.3		0.01	1289.3		0.01	1362.0		0.01			
$\sum h = \ln \beta_\Gamma$			11.42			8.39			9.43			7.90			8.52			9.63			
$\sum_{orphan} h$			1.24			1.27			1.19			1.23			1.03			1.24			
$\ln \beta_{exact}$			12.21			9.10			10.13			8.59			9.23			10.41			
$\overline{\chi}(\%)$		2.1			-8.2			-6.3			-9.1			-7.3			-3.4				-1.7
$\sigma(\chi)$		4.2			8.8			8.5			7.3			6.7			4.0				6.6
$\overline{\chi}^{h\,\dagger}$		5.5			-8.7			-4.0			-11.5			-8.4			-2.5				

$\dagger \overline{\chi}^h = \frac{\sum \chi \times h}{\sum h}$

(a) Carteret et al., 2013

Table EA-6: Modelled vibrational modes (frequencies in cm^{-1} and intensities) for grossular, and comparison to experiment. Measurements (Exp) are from Hofmeister and Chopelas (1991) for Raman, and McAloon and Hofmeister (1995) for Infrared. Question marks signal uncertain attributions. Values of $\ln\beta$ and h (in‰) are computed at 300K for the $^{44/40}$Ca pair. χ is the deviation (in %) betwenn the theoretical frequency and its experimental counterpart .

sym.	PZ: ν	PZ: χ (%)	PZ: h (‰)	PBE ν	PBE χ (%)	PBE h (‰)	vdW-DF2 ν	vdW-DF2 χ (%)	vdW-DF2 h (‰)	BLYP ν	BLYP χ (%)	BLYP h (‰)	BLYP+GD2 ν	BLYP+GD2 χ (%)	BLYP+GD2 h (‰)	PBESOL ν	PBESOL χ (%)	PBESOL h (‰)	Exp ν	B3LYP[(a)] ν	B3LYP[(a)] χ (%)
Raman																					
T_{2g}	**185.1**		**0.62**	**163.6**		**0.52**	**164.9**		**0.52**	**153.5**		**0.46**	**163.2**		**0.53**	**174.1**		**0.58**	**178?**	**176.6**	
T_{2g}	**242.0**	**1.7**	**0.49**	**218.9**	**-8.0**	**0.24**	**222.6**	**-6.5**	**0.11**	**213.6**	**-10.3**	**0.20**	**219.7**	**-7.7**	**0.31**	**229.7**	**-3.5**	**0.40**	**238**	**236.8**	**-0.5**
T_{2g}	**244.7**	**-0.5**	**0.37**	**225.3**	**-8.4**	**0.41**	**231.2**	**-6.0**	**0.58**	**223.5**	**-9.2**	**0.43**	**225.9**	**-8.2**	**0.36**	**233.8**	**-4.9**	**0.33**	**246**	**242.4**	**-1.5**
T_{2g}	**275.9**	**-0.7**	**0.56**	**260.6**	**-6.3**	**0.55**	**266.9**	**-4.0**	**0.46**	**261.5**	**-5.9**	**0.55**	**266.3**	**-4.2**	**0.54**	**266.6**	**-4.1**	**0.56**	**278**	**279.3**	**0.5**
T_{2g}	327.9	-0.6	0.14	309.1	-6.3	0.10	313.5	-5.0	0.13	307.5	-6.8	0.11	313.5	-5.0	0.08	317.1	-3.9	0.11	330	332.9	0.9
T_{2g}	349.1	0.0	0.00	331.9	-4.9	0.00	336.4	-3.6	0.00	331.7	-5.0	0.00	340.2	-2.5	0.00	338.9	-2.9	0.26	349	355.9	2.0
T_{2g}	**387.3**	**1.1**	**0.19**	**362.0**	**-5.5**	**0.11**	**366.9**	**-4.2**	**0.16**	**358.9**	**-6.3**	**0.16**	**368.1**	**-3.9**	**0.15**	**374.0**	**-2.3**	**0.17**	**383**	**390.0**	**1.8**
T_{2g}	471.3	-1.4	0.02	448.5	-6.2	0.01	460.5	-3.7	0.01	450.0	-5.9	0.01	460.1	-3.8	0.01	457.1	-4.4	0.02	478	483.1	1.1
T_{2g}	502.4	-1.3	0.04	485.6	-4.6	0.03	496.7	-2.4	0.03	488.9	-4.0	0.03	495.7	-2.6	0.03	490.8	-3.6	0.04	509	515.5	1.3
T_{2g}	567.0	-1.7	0.06	545.5	-5.5	0.03	558.5	-3.2	0.03	549.1	-4.8	0.03	558.7	-3.2	0.03	552.7	-4.2	0.04	577	586.5	1.6
T_{2g}	620.1	-1.4	0.04	598.4	-4.9	0.04	613.1	-2.5	0.03	603.6	-4.0	0.03	612.4	-2.6	0.03	605.3	-3.8	0.04	629	641.9	2.1
T_{2g}	823.8	-0.3	0.00	779.1	-5.7	0.01	763.3	-7.6	0.01	764.7	-7.4	0.01	783.0	-5.2	0.01	802.6	-2.8	0.00	826	814.7	-1.4
T_{2g}	846.5	-0.4	0.01	803.0	-5.5	0.01	785.5	-7.6	0.01	788.7	-7.2	0.01	805.2	-5.3	0.01	826.1	-2.8	0.01	850	839.8	-1.2
T_{2g}	997.2	-1.0	0.11	955.7	-5.1	0.11	948.6	-5.8	0.11	947.9	-5.9	0.11	964.3	-4.2	0.11	975.4	-3.1	0.11	1007	1007.3	0.0
A_{1g}	372.2	-0.5	0.00	347.4	-7.1	0.00	355.9	-4.8	0.00	343.2	-8.2	0.00	350.8	-6.2	0.00	358.1	-4.2	0.00	374	374.0	0.0
A_{1g}	546.8	-0.4	0.00	523.0	-4.7	0.00	534.3	-2.7	0.00	526.6	-4.1	0.00	536.4	-2.3	0.00	531.1	-3.3	0.00	549	562.8	2.5
A_{1g}	866.1	-1.7	0.00	830.6	-5.7	0.00	829.4	-5.9	0.00	826.2	-6.2	0.00	843.7	-4.2	0.00	846.7	-3.9	0.00	881	875.9	-0.6
E_g	**180.6**	**1.5**	**0.19**	**172.2**	**-3.2**	**0.18**	**176.2**	**-1.0**	**0.19**	**171.5**	**-3.6**	**0.18**	**177.0**	**-0.5**	**0.20**	**175.3**	**-1.5**	**0.19**	**178**	**184.7**	**3.8**
E_g	318.1	0.3	0.08	296.4	-6.5	0.09	299.1	-5.6	0.09	292.4	-7.7	0.10	297.5	-6.2	0.11	306.1	-3.4	0.08	317	322.5	1.7
E_g	**366.5**	**-0.7**	**0.28**	**344.5**	**-6.6**	**0.30**	**354.3**	**-4.0**	**0.31**	**343.9**	**-6.8**	**0.29**	**348.6**	**-5.5**	**0.32**	**353.8**	**-4.1**	**0.27**	**369**	**370.8**	**0.5**
E_g	**416.7**	**0.2**	**0.93**	**386.5**	**-7.1**	**0.67**	**396.1**	**-4.8**	**0.72**	**385.5**	**-7.3**	**0.64**	**392.3**	**-5.7**	**0.63**	**399.2**	**-4.0**	**0.79**	**416**	**422.4**	**1.5**
E_g	523.0	-0.6	0.02	499.9	-5.0	0.01	513.3	-2.4	0.01	503.9	-4.2	0.01	512.4	-2.6	0.01	507.5	-3.5	0.01	526	538.8	2.4
E_g	579.9	-1.7	0.05	562.1	-4.7	0.06	574.2	-2.7	0.05	565.6	-4.1	0.05	571.8	-3.1	0.05	568.4	-3.7	0.05	590	597.0	1.2
E_g	816.6		0.00	783.2		0.00	778.0		0.00	776.0		0.00	790.9		0.00	799.2		0.00	852?	823.2	
E_g	876.3		0.04	833.1		0.04	816.8		0.05	819.4		0.05	835.3		0.05	855.8		0.04	904?	872.1	
Infrared																					
T_{1u} TO	**154.6**	**-0.6**	**0.38**	**139.0**	**-10.7**	**0.33**	**143.0**	**-8.1**	**0.34**	**135.1**	**-13.2**	**0.31**	**133.6**	**-14.1**	**0.30**	**146.6**	**-5.8**	**0.35**	**155.6**	**153.4**	**-1.4**
T_{1u} LO	155.6	-1.2		141.2	-10.3		145.3	-7.7		138.7	-12.0		137.6	-12.6		148.1	-6.0		157.5	155.2	-1.5
T_{1u} TO	**183.3**	**-0.4**	**0.20**	**168.8**	**-8.3**	**0.32**	**172.4**	**-6.3**	**0.26**	**166.3**	**-9.6**	**0.24**	**169.7**	**-7.8**	**0.26**	**175.1**	**-4.8**	**0.15**	**184.0**	**183.7**	**-0.2**
T_{1u} LO	187.1	-0.9		173.8	-8.0		177.6	-6.0		171.6	-9.1		175.5	-7.0		179.3	-5.0		188.8	189.0	0.1
T_{1u} TO	**203.5**	**-0.5**	**0.46**	**192.1**	**-6.1**	**0.38**	**198.7**	**-2.8**	**0.35**	**193.4**	**-5.4**	**0.34**	**199.1**	**-2.7**	**0.36**	**195.9**	**-4.2**	**0.43**	**204.5**	**206.9**	**1.2**
T_{1u} LO	205.9	-0.7		194.1	-6.4		200.4	-3.4		195.0	-6.0		200.7	-3.2		198.4	-4.3		207.4	208.9	0.7
T_{1u} TO	**241.5**	**0.1**	**0.43**	**220.2**	**-8.8**	**0.37**	**222.0**	**-8.0**	**0.37**	**214.6**	**-11.1**	**0.36**	**223.2**	**-7.5**	**0.40**	**230.3**	**-4.6**	**0.40**	**241.4**	**242.0**	**0.2**
T_{1u} LO	247.4	-0.5		227.9	-8.4		230.2	-7.4		223.3	-10.2		233.5	-6.1		236.9	-4.7		248.7	248.0	-0.3
T_{1u} TO	**298.9**	**-0.6**	**0.48**	**277.7**	**-7.6**	**0.35**	**284.8**	**-5.3**	**0.38**	**275.9**	**-8.2**	**0.32**	**282.9**	**-5.9**	**0.33**	**286.6**	**-4.7**	**0.42**	**300.6**	**303.2**	**0.9**
T_{1u} LO	300.4	-0.8		278.9	-7.9		286.4	-5.5		277.4	-8.4		283.9	-6.3		287.8	-5.0		302.9	305.8	1.0
T_{1u} TO	**355.1**	**0.0**	**0.65**	**328.7**	**-7.4**	**0.56**	**329.7**	**-7.1**	**0.42**	**324.5**	**-8.6**	**0.48**	**334.1**	**-5.9**	**0.57**	**340.8**	**-4.0**	**0.36**	**355.0**	**357.5**	**0.7**
T_{1u} LO	355.7	-0.1		329.0	-7.6		329.8	-7.4		324.6	-8.8		334.7	-6.0		341.2	-4.1		356.0	357.8	0.5
T_{1u} TO	388.2	-0.4	0.14	361.8	-7.2	0.13	361.5	-7.3	0.11	355.8	-8.7	0.10	371.4	-4.7	0.07	373.6	-4.2	0.10	389.8	394.6	1.2
T_{1u} LO	397.1	-1.9		371.5	-8.2		374.9	-7.4		366.6	-9.5		381.0	-5.9		381.7	-5.7		404.9	406.7	0.4
T_{1u} TO	**397.5**		**0.21**	**374.5**		**0.22**	**382.7**		**0.25**	**375.7**		**0.27**	**383.3**		**0.25**	**382.9**		**0.21**		**407.0**	
T_{1u} LO	405.0			378.6			382.7			376.8			388.2			390.5				407.9	
T_{1u} TO	**414.6**	**-2.4**	**0.22**	**392.7**	**-7.6**	**0.20**	**394.0**	**-7.3**	**0.01**	**390.2**	**-8.2**	**0.09**	**404.5**	**-4.8**	**0.27**	**402.2**	**-5.4**	**0.21**	**425**	**424.2**	**-0.2**
T_{1u} LO	414.6	-7.9		392.9	-12.7		394.6	-12.3		390.2	-13.3		404.8	-10.0		402.3	-10.6		450	424.2	-5.7
T_{1u} TO	**440.2**	**1.2**	**0.73**	**408.9**	**-6.0**	**0.50**	**406.1**	**-6.6**	**0.90**	**401.4**	**-7.7**	**0.59**	**415.8**	**-4.4**	**0.38**	**424.0**	**-2.5**	**0.59**	**434.9**	**441.0**	**1.4**
T_{1u} LO	464.9	-1.0		441.3	-6.0		452.9	-3.5		443.2	-5.6		452.1	-3.7		449.9	-4.2		469.5	480.1	2.3
T_{1u} TO	466.3	-0.9	0.04	442.4	-6.0	0.04	453.0	-3.7	0.03	443.4	-5.8	0.04	452.9	-3.8	0.04	451.5	-4.0	0.03	470.6	480.8	2.2
T_{1u} LO	502.1	-0.8		481.7	-4.8		483.2	-4.5		478.7	-5.4		490.8	-3.0		490.6	-3.0		506.0	508.6	0.5
T_{1u} TO	502.0	-0.8	0.03	482.0	-4.7	0.03	486.7	-3.8	0.04	480.5	-5.0	0.03	491.4	-2.9	0.03	490.6	-3.0	0.03	506.0	509.3	0.7

Table EA-6: (continued)

sym.	PZ: ν	χ (%)	h (‰)	PBE ν	χ (%)	h (‰)	vdW-DF2 ν	χ (%)	h (‰)	BLYP ν	χ (%)	h (‰)	BLYP+GD2 ν	χ (%)	h (‰)	PBESOL ν	χ (%)	h (‰)	Exp. ν	B3LYP[(a)] ν	χ (%)
T_{1u} LO	528.3	-0.2		504.6	-4.7		509.0	-3.9		503.1	-5.0		515.1	-2.7		514.7	-2.8		529.4	539.2	1.9
T_{1u} TO	537.9	-0.3	0.15	514.0	-4.8	0.12	515.8	-4.4	0.13	510.2	-5.5	0.12	523.7	-3.0	0.14	524.9	-2.8	0.14	539.8	546.4	1.2
T_{1u} LO	574.3	-0.3		544.7	-5.5		542.5	-5.8		538.1	-6.6		551.1	-4.4		558.9	-3.0		576.2	583.1	1.2
T_{1u} TO	609.4	-1.4	0.09	587.3	-5.0	0.10	594.8	-3.7	0.08	587.4	-5.0	0.09	598.1	-3.2	0.09	596.1	-3.5	0.10	618.0	625.9	1.3
T_{1u} LO	615.4	-1.4		592.4	-5.0		603.3	-3.3		594.6	-4.7		604.3	-3.1		600.9	-3.7		623.8	634.4	1.7
T_{1u} TO	835.4	-0.3	0.01	793.2	-5.3	0.01	778.8	-7.0	0.01	780.9	-6.8	0.01	797.8	-4.8	0.01	814.9	-2.7	0.01	837.7	829.6	-1.0
T_{1u} LO	849.0	-0.3		806.7	-5.2		793.5	-6.8		795.0	-6.6		812.2	-4.6		828.3	-2.7		851.4	845.6	-0.7
T_{1u} TO	854.1	-0.3	0.02	811.2	-5.3	0.02	797.4	-6.9	0.03	799.1	-6.7	0.03	816.6	-4.6	0.03	833.2	-2.7	0.02	856.3	849.6	-0.8
T_{1u} LO	882.4	-0.3		839.0	-5.2		824.6	-6.8		826.7	-6.6		844.2	-4.6		861.0	-2.7		884.7	879.8	-0.6
T_{1u} TO	902.8	-0.5	0.08	860.9	-5.2	0.08	846.3	-6.8	0.09	848.9	-6.5	0.09	864.9	-4.7	0.08	882.3	-2.8	0.08	907.8	901.8	-0.7
T_{1u} LO	991.2	-1.6		948.5	-5.8		940.8	-6.6		939.7	-6.7		954.3	-5.3		969.0	-3.8		1007.4	1002.5	-0.5
Silent																					
T_{2u}	**162.1**	**0.39**		**147.1**	**0.37**		**147.7**	**0.38**		**140.4**	**0.36**		**144.6**	**0.37**		**153.8**	**0.38**				
T_{2u}	**191.7**	**0.39**		**182.1**	**0.32**		**184.3**	**0.33**		**182.1**	**0.31**		**180.2**	**0.34**		**185.4**	**0.34**				
T_{2u}	**249.6**	**0.53**		**232.0**	**0.46**		**236.8**	**0.45**		**230.7**	**0.45**		**236.0**	**0.43**		**238.9**	**0.48**				
T_{2u}	295.9	0.14		283.6	0.10		291.2	0.09		283.9	0.07		293.0	0.06		287.8	0.13				
T_{2u}	**314.9**	**0.29**		**290.6**	**0.21**		**298.1**	**0.22**		**289.1**	**0.20**		**297.1**	**0.20**		**300.6**	**0.24**				
T_{2u}	329.0	0.06		313.0	0.02		315.0	0.01		311.5	0.00		321.9	0.02		319.6	0.04				
T_{2u}	**354.0**	**0.30**		**327.3**	**0.22**		**330.3**	**0.17**		**321.0**	**0.17**		**333.7**	**0.17**		**339.5**	**0.27**				
T_{2u}	**401.3**	**0.20**		**377.0**	**0.16**		**377.8**	**0.19**		**372.3**	**0.17**		**383.0**	**0.15**		**387.9**	**0.17**				
T_{2u}	439.6	0.03		412.0	0.04		409.2	0.08		405.3	0.06		422.0	0.06		425.2	0.03				
T_{2u}	465.7	0.07		437.2	0.09		427.5	0.11		426.7	0.11		446.9	0.12		451.7	0.07				
T_{2u}	514.5	0.06		490.9	0.05		500.0	0.05		492.3	0.05		502.4	0.06		499.8	0.06				
T_{2u}	587.0	0.07		560.4	0.05		565.2	0.04		558.5	0.04		571.5	0.05		571.8	0.06				
T_{2u}	600.9	0.09		577.5	0.09		589.3	0.10		580.9	0.10		592.2	0.10		586.0	0.09				
T_{2u}	826.1	0.02		788.8	0.02		777.5	0.02		778.2	0.02		794.6	0.02		807.7	0.02				
T_{2u}	869.6	0.02		829.2	0.02		822.5	0.02		820.2	0.02		837.5	0.02		848.9	0.02				
T_{2u}	889.6	0.06		847.6	0.06		839.3	0.07		838.0	0.07		856.3	0.07		868.1	0.06				
T_{1g}	**185.0**	**0.63**		**171.0**	**0.45**		**171.8**	**0.53**		**166.6**	**0.57**		**173.5**	**0.62**		**177.6**	**0.63**				
T_{1g}	**194.3**	**0.69**		**174.4**	**0.55**		**178.9**	**0.56**		**170.7**	**0.45**		**175.7**	**0.51**		**183.9**	**0.63**				
T_{1g}	**235.6**	**0.24**		**214.5**	**0.19**		**213.0**	**0.26**		**208.6**	**0.23**		**215.0**	**0.20**		**224.6**	**0.20**				
T_{1g}	288.0	0.13		271.9	0.03		276.0	0.04		269.6	0.05		277.2	0.10		278.6	0.08				
T_{1g}	**300.6**	**0.53**		**279.3**	**0.58**		**284.7**	**0.46**		**276.8**	**0.44**		**281.1**	**0.44**		**289.0**	**0.56**				
T_{1g}	**330.0**	**1.25**		**307.2**	**1.12**		**315.6**	**1.36**		**306.7**	**1.28**		**310.0**	**1.25**		**316.6**	**1.15**				
T_{1g}	380.0	0.07		360.4	0.05		369.1	0.04		362.3	0.04		368.0	0.05		367.3	0.06				
T_{1g}	**408.0**	**0.32**		**383.1**	**0.21**		**394.5**	**0.22**		**384.7**	**0.18**		**390.8**	**0.18**		**392.4**	**0.26**				
T_{1g}	**460.5**	**0.20**		**442.4**	**0.14**		**454.8**	**0.15**		**445.7**	**0.13**		**452.8**	**0.13**		**448.5**	**0.17**				
T_{1g}	488.3	0.04		470.8	0.01		482.7	0.02		473.4	0.01		480.8	0.01		476.3	0.02				
T_{1g}	**560.9**	**0.40**		**535.5**	**0.30**		**545.8**	**0.30**		**536.8**	**0.28**		**546.4**	**0.29**		**544.9**	**0.35**				
T_{1g}	810.0	0.00		765.7	0.00		748.4	0.00		750.9	0.00		768.7	0.00		789.1	0.00				
T_{1g}	833.9	0.11		799.6	0.10		795.2	0.11		792.6	0.10		808.1	0.10		815.8	0.10				
T_{1g}	921.2	0.10		879.9	0.10		870.4	0.10		870.8	0.10		888.0	0.10		900.0	0.09				
E_u	234.9	0.07		220.3	0.07		222.2	0.13		217.9	0.08		223.3	0.09		226.8	0.07				
E_u	**300.0**	**0.82**		**276.5**	**0.70**		**283.9**	**0.70**		**275.8**	**0.67**		**281.4**	**0.73**		**286.6**	**0.76**				
E_u	330.0	0.03		310.2	0.03		312.9	0.06		307.3	0.04		319.3	0.01		318.5	0.02				
E_u	**390.1**	**0.31**		**366.7**	**0.22**		**374.0**	**0.22**		**364.1**	**0.22**		**371.4**	**0.21**		**376.5**	**0.26**				
E_u	419.8	0.03		395.7	0.06		399.4	0.14		395.7	0.10		407.4	0.08		405.4	0.04				
E_u	454.1	0.01		428.6	0.02		423.9	0.01		420.4	0.02		434.6	0.02		441.3	0.01				
E_u	**550.5**	**0.26**		**525.2**	**0.21**		**536.4**	**0.18**		**526.8**	**0.18**		**538.4**	**0.19**		**534.5**	**0.24**				
E_u	630.1	0.14		605.2	0.11		617.2	0.12		608.1	0.11		617.5	0.11		614.2	0.12				
E_u	851.9	0.10		816.7	0.09		811.0	0.10		809.1	0.09		824.9	0.09		833.5	0.09				
E_u	884.1	0.00		843.0	0.00		826.8	0.00		830.4	0.00		845.5	0.00		864.4	0.00				
A_{1u}	300.6	0.00		285.0	0.00		288.1	0.00		283.0	0.00		295.1	0.00		291.8	0.00				
A_{1u}	378.6	0.00		361.0	0.00		370.1	0.00		362.9	0.00		371.9	0.00		367.4	0.00				
A_{1u}	460.8	0.00		435.9	0.00		439.7	0.00		432.0	0.00		444.1	0.00		446.6	0.00				
A_{1u}	652.7	0.00		624.6	0.00		627.4	0.00		621.6	0.00		633.5	0.00		637.1	0.00				
A_{1u}	976.7	0.00		933.1	0.00		926.3	0.00		924.9	0.00		940.4	0.00		953.9	0.00				
A_{2u}	189.9	0.04		179.2	0.04		187.3	0.04		179.8	0.04		180.0	0.04		182.8	0.03				
A_{2u}	**294.3**	**0.39**		**274.7**	**0.36**		**282.2**	**0.37**		**274.3**	**0.35**		**276.4**	**0.36**		**282.8**	**0.37**				
A_{2u}	**440.1**	**0.31**		**413.2**	**0.23**		**420.1**	**0.26**		**412.1**	**0.23**		**421.6**	**0.22**		**423.9**	**0.26**				
A_{2u}	482.4	0.00		460.5	0.01		460.6	0.00		457.4	0.00		470.8	0.01		470.5	0.01				
A_{2u}	845.3	0.00		808.9	0.00		804.6	0.00		801.8	0.00		819.8	0.00		826.2	0.00				
A_{2g}	201.0	0.14		190.9	0.13		196.1	0.14		191.5	0.14		195.2	0.14		194.7	0.13				
A_{2g}	**376.8**	**0.38**		**346.3**	**0.24**		**357.5**	**0.36**		**344.3**	**0.32**		**348.8**	**0.32**		**359.3**	**0.35**				
A_{2g}	440.0	0.20		417.2	0.14		428.9	0.14		418.3	0.14		424.5	0.14		425.9	0.16				
A_{2g}	562.3	0.00		544.5	0.00		555.2	0.00		548.3	0.00		556.0	0.00		550.2	0.00				
A_{2g}	968.7	0.03		927.7	0.03		916.0	0.03		918.0	0.03		934.2	0.03		947.8	0.03				
$\sum h = \ln \beta_\Gamma$		19.25			16.08			16.89			15.79			16.19			17.44				
$\sum_{orphan} h$		11.56			9.58			10.30			9.60			9.84			10.54				
$\ln \beta_{exact}$		19.36			16.28			17.06			15.93			16.36			17.61				

Table EA-6: (continued)

sym.	PZ: ν	χ (%)	h (‰)	PBE ν	χ (%)	h (‰)	vdW-DF2 ν	χ (%)	h (‰)	BLYP ν	χ (%)	h (‰)	BLYP+GD2 ν	χ (%)	h (‰)	PBESOL ν	χ (%)	h (‰)	Exp. ν	B3LYP[(a)] ν	χ (%)
$\overline{\chi}$		-0.7			-6.4			-5.4			-7.1			-5.0			-3.9				0.5
$\sigma(\chi)$		1.3			1.8			2.1			2.3			2.4			1.3				1.5
$\overline{\chi}^{h\,\dagger}$		-0.1			-7.0			-5.5			-7.8			-5.7			-3.9				

$\dagger \overline{\chi}^h = \frac{\sum \chi \times h}{\sum h}$

(a) Zicovich-Wilson et al. (2008) for infrared, Dovesi et al. (2009) for Raman

Table EA-7: Modelled vibrational modes (frequencies and intensities) for diopside, and comparison to experiment. Measurements (Exp) correspond to typical values compiled from Etchepare (1972), Swamy et al. (1997), Chopelas and Serghiou (2002) and Prencipe (2012) for Raman, and are taken from Zulumyan et al. (1976) for Infrared. . Values of lnβ and h (in‰) are computed at 300K for the $^{44/40}$Ca pair. χ is the deviation (in %) betwenn the theoretical frequency and its experimental counterpart.

Raman

sym.	PZ: ν	χ (%)	h (‰)	PBE ν	χ (%)	h (‰)	vdW-DF2 ν	χ (%)	h (‰)	BLYP ν	χ (%)	h (‰)	BLYP+GD2 ν	χ (%)	h (‰)	PBESOL ν	χ (%)	h (‰)	Exp ν	B3LYP[(a)] ν	χ (%)
A_g	138.6	-1.0	0.01	121.9	-12.9	0.02	127.7	-8.8	0.00	115.5	-17.5	0.03	123.1	-12.1	0.00	129.6	-7.5	0.02	140	137	
A_g	**182.5**	**0.3**	**0.85**	**170.7**	**-6.2**	**0.77**	**173.6**	**-4.6**	**0.85**	**168.0**	**-7.7**	**0.71**	**172.6**	**-5.2**	**0.84**	**175.7**	**-3.4**	**0.80**	**182**	**180**	
A_g	234.0	0.0	0.05	221.2	-5.5	0.06	234.8	0.4	0.11	222.4	-4.9	0.09	234.1	0.0	0.00	224.8	-3.9	0.05	234	235	
A_g	**250.6**	**-2.1**	**0.38**	**237.5**	**-7.2**	**0.44**	**242.6**	**-5.2**	**0.39**	**235.5**	**-8.0**	**0.47**	**245.7**	**-4.0**	**0.47**	**242.6**	**-5.2**	**0.42**	**256**	**253**	
A_g	**314.6**	**1.5**	**0.87**	**293.6**	**-5.3**	**0.41**	**299.6**	**-3.4**	**0.32**	**283.0**	**-8.7**	**0.08**	**302.5**	**-2.4**	**0.48**	**301.6**	**-2.7**	**0.66**	**310**	**307**	
A_g	325.9	-0.0	0.06	304.0	-6.8	0.11	309.8	-5.0	0.19	299.8	-8.0	0.38	315.9	-3.1	0.10	314.9	-3.4	0.04	326	321	
A_g	369.3	2.6	0.01	335.3	-6.9	0.01	337.9	-6.1	0.02	328.5	-8.7	0.00	342.6	-4.8	0.04	351.4	-2.4	0.01	360	351	
A_g	396.9	1.8	0.04	368.6	-5.5	0.02	375.7	-3.7	0.01	365.1	-6.4	0.02	379.6	-2.7	0.03	379.9	-2.6	0.03	390	387	
A_g	498.0	-2.0	0.00	481.7	-5.2	0.01	497.5	-2.1	0.01	485.9	-4.4	0.00	494.6	-2.6	0.01	486.1	-4.3	0.01	508	518	
A_g	526.3	-0.7	0.04	507.0	-4.3	0.02	517.2	-2.4	0.01	510.3	-3.7	0.02	518.3	-2.2	0.03	513.0	-3.2	0.03	530	535	
A_g	**652.5**	**-2.2**	**0.29**	**626.9**	**-6.0**	**0.25**	**635.9**	**-4.7**	**0.27**	**627.0**	**-6.0**	**0.25**	**641.6**	**-3.8**	**0.29**	**636.7**	**-4.5**	**0.27**	**667**	**671**	
A_g	849.0	-0.8	0.00	813.9	-4.9	0.00	794.1	-7.2	0.00	810.4	-5.3	0.00	817.1	-4.5	0.00	830.6	-3.0	0.00	856	850	
A_g	998.0	-1.6	0.10	958.1	-5.5	0.10	956.6	-5.7	0.10	950.3	-6.3	0.10	966.4	-4.7	0.10	976.5	-3.7	0.10	1014	1007	
A_g	1031.7	-1.6	0.02	988.0	-5.7	0.02	985.3	-6.0	0.03	976.5	-6.8	0.02	992.4	-5.3	0.02	1009.0	-3.7	0.02	1048	1038	
B_g	**116.6**	**1.4**	**0.44**	**105.6**	**-8.2**	**0.40**	**114.5**	**-0.5**	**0.46**	**104.3**	**-9.3**	**0.40**	**117.2**	**1.9**	**0.44**	**110.1**	**-4.3**	**0.42**	**115**	**116**	
B_g	159.7	-3.2	0.12	153.0	-7.3	0.07	166.3	0.8	0.14	155.0	-6.1	0.07	167.0	1.2	0.17	153.2	-7.1	0.09	165	167	
B_g	**192.7**	**-1.7**	**0.64**	**181.4**	**-7.5**	**0.61**	**186.9**	**-4.7**	**0.69**	**179.0**	**-8.7**	**0.60**	**190.0**	**-3.1**	**0.83**	**185.7**	**-5.3**	**0.60**	**196**	**196**	
B_g	**230.4**	**0.2**	**0.92**	**215.0**	**-6.5**	**0.65**	**220.2**	**-4.3**	**0.53**	**213.2**	**-7.3**	**0.48**	**221.1**	**-3.9**	**0.53**	**221.2**	**-3.8**	**0.81**	**230**	**229**	
B_g	301.8	-0.4	0.11	285.3	-5.8	0.07	292.1	-3.6	0.05	282.6	-6.7	0.80	289.1	-4.6	0.14	291.6	-3.8	0.09	303	305	
B_g	**336.1**	**8.4**	**0.88**	**297.2**	**-4.1**	**0.73**	**298.1**	**-3.8**	**0.81**	**284.1**	**-8.4**	**0.12**	**307.1**	**-0.9**	**0.65**	**316.7**	**2.2**	**0.76**	**310**	**311**	
B_g	360.5	1.0	0.20	335.1	-6.1	0.19	344.7	-3.4	0.20	332.0	-7.0	0.23	349.4	-2.1	0.21	345.8	-3.1	0.17	357	356	
B_g	368.3	0.4	0.03	351.1	-4.3	0.04	359.3	-2.1	0.03	350.9	-4.4	0.02	358.7	-2.3	0.01	356.6	-2.8	0.06	367	370	
B_g	**392.8**	**-0.0**	**0.40**	**372.3**	**-5.3**	**0.36**	**383.0**	**-2.5**	**0.45**	**373.5**	**-5.0**	**0.43**	**381.6**	**-2.9**	**0.34**	**379.3**	**-3.5**	**0.35**	**393**	**396**	
B_g	471.1	1.1	0.08	443.7	-4.8	0.08	448.7	-3.7	0.07	439.5	-5.7	0.09	453.0	-2.8	0.12	455.4	-2.3	0.08	466	463	
B_g	507.1	-1.5	0.08	487.2	-5.4	0.05	496.7	-3.5	0.06	486.9	-5.5	0.03	497.6	-3.4	0.08	494.1	-4.1	0.06	515	517	
B_g	**549.3**	**-1.9**	**0.42**	**527.7**	**-5.8**	**0.39**	**545.4**	**-2.6**	**0.41**	**530.3**	**-5.3**	**0.41**	**543.7**	**-2.9**	**0.41**	**534.7**	**-4.5**	**0.40**	**560**	**569**	
B_g	698.9	-1.4	0.10	673.7	-5.0	0.09	676.9	-4.5	0.10	673.4	-5.0	0.09	685.2	-3.4	0.10	683.8	-3.5	0.10	709	715	
B_g	897.7	-2.1	0.00	856.4	-6.6	0.00	853.9	-6.9	0.00	845.8	-7.8	0.00	862.6	-5.9	0.00	876.4	-4.4	0.00	917	901	
B_g	958.3	-0.9	0.06	924.2	-4.4	0.07	913.0	-5.6	0.07	923.1	-4.5	0.07	931.2	-3.7	0.07	939.3	-2.9	0.06	967	971	
B_g	1037.9	-1.0	0.04	994.3	-5.1	0.04	990.4	-5.5	0.04	983.8	-6.1	0.04	998.3	-4.7	0.05	1015.0	-3.2	0.04	1048	1042	

Infrared

sym.	PZ: ν	χ (%)	h (‰)	PB: ν	χ (%)	h (‰)	PBV: ν	χ (%)	h (‰)	BL: ν	χ (%)	h (‰)	BLV: ν	χ (%)	h (‰)	PBESOL: ν	χ (%)	h (‰)	Exp ν	B3LYP[(a)] ν	χ (%)
A_u	**214.5**	**-2.5**	**0.16**	**202.4**	**-8.0**	**0.84**	**208.1**	**-5.4**	**1.02**	**198.9**	**-9.6**	**0.95**	**207.1**	**-5.8**	**0.68**	**207.6**	**-5.6**	**0.43**	**220**		
A_u	**235.8**	**-1.7**	**1.53**	**217.8**	**-9.2**	**0.52**	**223.6**	**-6.8**	**0.40**	**218.3**	**-9.1**	**0.32**	**226.4**	**-5.7**	**0.81**	**224.1**	**-6.6**	**1.08**	**240**		
A_u	305.8	0.3	0.04	291.2	-4.5	0.04	299.7	-1.7	0.03	291.5	-4.4	0.10	295.7	-3.0	0.02	296.0	-3.0	0.03	305		
A_u	357.0	6.6	0.12	315.4	-5.8	0.16	314.6	-6.1	0.16	297.5	-11.2	0.16	324.6	-3.1	0.12	338.0	0.9	0.14	335		
A_u	365.1	0.6	0.02	349.4	-3.7	0.00	354.4	-2.4	0.00	352.8	-2.8	0.00	350.6	-3.4	0.01	353.0	-2.8	0.00	363		
A_u	**409.3**	**-0.2**	**0.42**	**390.7**	**-4.7**	**0.26**	**400.9**	**-2.2**	**0.26**	**390.0**	**-4.9**	**0.24**	**406.6**	**-0.8**	**0.34**	**397.2**	**-3.1**	**0.33**	**410**		
A_u	468.4	0.7	0.01	447.8	-3.7	0.02	458.7	-1.4	0.02	447.6	-3.7	0.02	459.5	-1.2	0.03	455.2	-2.1	0.02	465		
A_u	493.7	-2.2	0.00	472.6	-6.4	0.00	488.4	-3.3	0.01	473.0	-6.3	0.00	484.9	-4.0	0.02	479.6	-5.0	0.00	505		
A_u	507.2		0.00	487.8		0.00	502.0		0.00	490.1		0.00	503.9		0.00	493.7		0.00			
A_u	663.1	-1.0	0.02	644.4	-3.8	0.03	639.6	-4.5	0.02	646.4	-3.5	0.03	648.7	-3.2	0.02	651.7	-2.7	0.02	670		
A_u	899.0	-1.7	0.00	855.7	-6.5	0.00	852.4	-6.8	0.00	843.6	-7.8	0.00	862.5	-5.7	0.00	877.1	-4.1	0.00	915		
A_u	945.9	-1.5	0.00	912.4	-5.0	0.00	902.6	-6.0	0.00	911.9	-5.0	0.00	920.1	-4.2	0.00	927.1	-3.4	0.00	960		
A_u	1056.8	-1.2	0.01	1014.7	-5.2	0.01	1012.2	-5.4	0.01	1005.2	-6.1	0.01	1019.4	-4.7	0.01	1034.4	-3.3	0.01	1070		
B_u	**138.6**		**0.48**	**128.0**		**0.46**	**138.8**		**0.54**	**120.4**		**0.32**	**140.1**		**0.46**	**133.2**		**0.48**			
B_u	172.1		0.13	150.1		0.08	158.7		0.09	147.8		0.20	157.7		0.18	159.4		0.08			
B_u	**269.5**		**0.57**	**249.4**		**0.50**	**253.4**		**0.51**	**244.8**		**0.52**	**257.7**		**0.61**	**257.7**		**0.52**			
B_u	**292.5**	**3.7**	**2.36**	**271.9**	**-3.6**	**1.73**	**279.6**	**-0.9**	**1.54**	**268.4**	**-4.8**	**1.09**	**277.7**	**-1.5**	**1.87**	**281.3**	**-0.3**	**2.19**	**282**		
B_u	**304.8**	**3.3**	**0.08**	**286.2**	**-3.0**	**0.40**	**291.2**	**-1.3**	**0.64**	**285.6**	**-3.2**	**1.00**	**293.1**	**-0.6**	**0.29**	**293.6**	**-0.5**	**0.10**	**295**		
B_u	322.7	-0.7	0.23	307.7	-5.3	0.05	314.6	-3.2	0.09	309.5	-4.8	0.06	315.8	-2.8	0.11	312.1	-4.0	0.10	325		

Table EA-7: (continued)

B_u	384.8	-0.0	0.21	349.4	-9.2	0.21	353.5	-8.2	0.22	340.2	-11.6	0.23	360.8	-6.3	0.14	365.8	-5.0	0.20	385
B_u	431.2	0.3	0.03	405.5	-5.7	0.02	408.8	-4.9	0.03	399.1	-7.2	0.02	412.5	-4.1	0.02	416.6	-3.1	0.02	430
B_u	445.1	-2.2	0.01	426.9	-6.2	0.00	438.8	-3.6	0.00	430.4	-5.4	0.00	434.9	-4.4	0.01	432.7	-4.9	0.01	455
B_u	509.9	-1.0	0.06	490.5	-4.7	0.06	500.6	-2.8	0.06	492.8	-4.3	0.06	501.1	-2.7	0.06	497.1	-3.5	0.06	515
B_u	618.8	-1.8	0.15	595.5	-5.5	0.14	601.2	-4.6	0.14	594.2	-5.7	0.14	608.2	-3.5	0.17	605.0	-4.0	0.14	630
B_u	847.1	-1.5	0.00	812.0	-5.6	0.00	792.4	-7.9	0.00	808.7	-6.0	0.00	815.4	-5.2	0.00	828.7	-3.6	0.00	860
B_u	948.7	-2.7	0.04	907.1	-7.0	0.04	903.3	-7.4	0.04	895.9	-8.1	0.04	911.4	-6.5	0.04	927.5	-4.9	0.04	975
B_u	1042.2	-1.7	0.00	999.4	-5.7	0.01	996.8	-6.0	0.00	989.8	-6.6	0.01	1004.1	-5.3	0.01	1019.6	-3.8	0.00	1060
$\sum h = \ln \beta_\Gamma$			13.92			11.66			12.25			11.57			12.59			12.55	
$\sum_{orphan} h$			1.18			1.04			1.14			1.04			1.25			1.08	
$\ln \beta_{exact}$			14.86			12.53			13.17			12.45			13.53			13.45	
$\overline{\chi}$		-0.3			-5.8			-4.2			-6.6			-3.6			-3.6		
$\sigma(\chi)$		2.2			1.7			2.2			2.5			2.2			1.7		
$\overline{\chi}^{h\,\dagger}$		0.9			-5.9			-3.5			-6.8			-3.0			-3.1		

$\dagger \overline{\chi}^h = \frac{\sum \chi \times h}{\sum h}$

Althoff P. (1977) Structural refinements of dolomite and a magnesian calcite and implications for dolomite formation in the marine environment. *American Mineralogist* **62**, 772–783.

Böttcher M.E., Gehlken P.L. and Steele D. (1997) Characterization of inorganic and biogenic magnesian calcites by Fourier Transform infrared spectroscopy. *Solid State Ionics* **101-103**, 1379–1385. International Symposium on the Reactivity of Solids.

Cameron M., Sueno S., Prewitt C.T. and Papike J.J. (1973) High-temperature crystal chemistry of acmite, diopside, hedenbergite, jadeite,spodumene, and ureyite. *American Mineralogist* **58**, 594–618.

Carteret C., De La Pierre M., Dossot M., Pascale F., Erba A. and Dovesi R. (2013) The vibrational spectrum of CaCO3 aragonite: a combined experimental and quantum-mechanical investigation. *The Journal of chemical physics* **138**, 014201.

Caspi E.N., Pokroy B., Lee P.L., Quintana J.P. and Zolotoyabko E. (2005) On the structure of aragonite. *Acta Crystallographica Section B* **61**, 129–132.

Chopelas A. and Serghiou G. (2002) Spectroscopic evidence for pressure-induced phase transitions in diopside **29**, 403–408.

De La Pierre M., Demichelis R. and Dovesi R. (2016) *Vibrational Spectroscopy of Minerals Through Ab Initio Methods*, John Wiley & Sons, Ltd, chapter 10. pp. 341–374.

Deines P. (2004) Carbon isotope effects in carbonate systems1 1Associate editor: S. M. F. Sheppard. *Geochimica et Cosmochimica Acta* **68**, 2659 – 2679.

Dovesi R., Valenzano L., Pascale F., Zicovich-Wilson C.M. and Orlando R. (2009) Ab initio quantum-mechanical simulation of the Raman spectrum of grossular. *Journal of Raman Spectroscopy* **40**, 416–418.

Effenberger H., Mereiter K. and Zemann J. (1981) Crystal structure refinements of magnesite, calcite, rhodochrosite, siderite, smithonite, and dolomite, with discussion of some aspects of the stereochemistry of calcite type carbonates. *Zeitschrift für Kristallographie - Crystalline Materials* **156**, 233 – 244.

Erba A., Shahrokhi M., Moradian R. and Dovesi R. (2015) On how differently the quasi-harmonic approximation works for two isostructural crystals: Thermal properties of periclase and lime. *The Journal of Chemical Physics* **142**, 044114.

Etchepare J. (1972) *Amorphous materials international conference on noncrystalline solids*, Wiley Interscience, London, chapter Study by Raman spectroscopy of crystalline and glassy diopside. pp. 337–346.

Geiger C.A. and Armbruster T. (1997) $Mn_3Al_2Si_3O_{12}$ spessartine and $Ca_3Al_2Si_3O_{12}$ grossular garnet: structural dynamic and thermodynamic properties. *Am. Mineral.* **82**, 740–747.

Gillet P., Biellmann C., Reynard B. and McMillan P. (1993) Raman spectroscopic studies of carbonates part I: High-pressure and high-temperature behaviour of calcite, magnesite, dolomite and aragonite. *Physics and Chemistry of Minerals* **20**, 1–18.

Gillet P., McMillan P., Schott J., Badro J. and Grzechnik A. (1996) Thermodynamic properties and isotopic fractionation of calcite from vibrational spectroscopy of 18O-substituted calcite. *Geochimica et Cosmochimica Acta* **60**, 3471 – 3485.

Hellwege K., Lesch W., Plihal M. and Schaack G. (1970) Zwei-phononen-absorptionsspektren und dispersion der schwingungszweige in kristallen der kalkspatstruktur. *Zeitschrift für Physik A Hadrons and nuclei* **232**, 61–86.

Hofmeister A. and Chopelas A. (1991) Vibrational spectroscopy of end-member silicate garnets. *Physics and Chemistry of Minerals* **17**, 503–526.

Matas J., Gillet P., Ricard Y. and Martinez I. (2000) Thermodynamic properties of carbonates at high pressures from vibrational modelling. *European Journal of Mineralogy* **12**, 703–720.

McAloon B.P. and Hofmeister A.M. (1995) Single-crystal IR spectroscopy of grossular-andradite garnets. *American Mineralogist* **80**, 1145–1156.

Prencipe M. (2012) Simulation of vibrational spectra of crystals by ab initio calculations: an invaluable aid in the assignment and interpretation of the Raman signals. The case of jadeite $NaAlSi_2O_6$. *Journal of raman spectroscopy* **43**, 1567–1569.

Rieder K.H., Weinstein B.A., Cardona M. and Bilz H. (1973) Measurement and Comparative Analysis of the Second-Order Raman Spectra of the Alkaline-Earth Oxides with a NaCl Structure. *Phys. Rev. B* **8**, 4780–4786.

Saunderson D.H. and Peckham G.E. (1971) The lattice dynamics of calcium oxide. *Journal of Physics C: Solid State Physics* **4**, 2009–2016.

Speziale S., Shieh S.R. and Duffy T.S. (2006) High-pressure elasticity of calcium oxide: A comparison between Brillouin spectroscopy and radial X-ray diffraction. *Journal of Geophysical Research: Solid Earth* **111**.

Swamy V., Dubrovinsky L.S. and Martsui M. (1997) High-temperature Raman spectroscopy and quasi-harmonic lattice dynamic simulation of diopside **24**, 440–446.

Valenzano L., Noël Y., Orlando R., Zicovich-Wilson C.M., Ferrero M. and Dovesi R. (2007) Ab initio vibrational spectra and dielectric properties of carbonates: magnesite, calcite and dolomite. *Theoretical Chemistry Accounts* **117**, 991–1000.

Vijayaraghavan P., Marsongkohadi X. and Iyengar P. (1972) In *Proceedings of Symposium on Neutron Inelastic Scattering, Genoble, France, 1972*.

Zicovich-Wilson C.M., Torres F.J., Pascale F., Valenzano L., Orlando R. and Dovesi R. (2008) Ab initio simulation of the IR spectra of pyrope, grossular, and andradite. *Journal of Computational Chemistry* **29**, 2268–2278.

Zulumyan N.O., Mirgorodskii A., Pavinich V. and Lazarev A. (1976) Study of calculation of the vibrational spectrum of a crystal with complex polyatomic anions. Diopside $CaMgSi_2O_6$. *Optics and spectrometry* **41**, 622–627.